D-meson production according to the parton model and their detection in ALICE

Tuomo Kalliokoski

August 16, 2007

Abstract

Modern understanding in particle physics is constructed over layers and layers of work. Most of the work was done during last century, starting from the quantum mechanics. Modern theoretical basis is the parton model, which is constructed from three independent parts: distribution of momentum to partons inside hadron, partonic cross-sections from QCD and from fragmentation of parton to hadrons. All of these parts are discussed in this work. Future experiments are aiming for higher energies and/or greater number of intresting events than what previous experiments were capable to gain. Main example of this is LHC and ALICE-experiment on it in CERN. While simulations have benefited greatly from fast increase of computing power during last few decades.

With the following assumptions, $p_t > 1GeV$, fixed QCD scale $Q = 5GeV$, massless quarks and only gluon-gluon channel in partonic cross-section and δ-function fragmentation, the lowest order simulations for production of D-meson with midrapidity $y = 0$ and rapidity interval $\Delta y = 1$ at proton-proton collision predicts that 51% of D^0 and 76% of D^+ decay at transverse distance $l > 60\mu m$ from the main interaction point and thus ALICE is capable of detecting them from reconstructed tracks of their decay products. With same assumptions production rate of D-mesons in prime interaction in ALICE is 108 000 000 in one hour. 3/4 of them are on excited states D^* and of the rest half are charged D^+-mesons and half are neutral D^0-mesons. This sums up into 6 890 000 D^0 and 10 300 000 D^+ events from primary D-mesons are available to detection in one hour of operation in LHC.

Preface

The author would like to thank the members of JYFL staff and especially the supervisors of the work Vesa Ruuskanen and Wladyslaw Trzaska for help and guidance in this work.

Contents

List of Figures

List of Tables

1 Introduction

Life and Quarks[1]

> There are ups and downs in life.
> Sometimes it's even strange and it can be charming.
> One should never forget the bottom line: Beauty of physics.
> Which is the truth at the top.

Particle physics is one of the most active and expensive fields of today's research in physics. Like every other field of study it can be divided in multiple ways, but in this work it is divided in three ways: theoretical, simulational and experimental fields of study. From the theory we get predictions which are included in simulations of future empirical experiments. The history of particle physics is very closely bound with advances in quantum mechanics, even though first experiments on particle and nuclear physics[2] were made before the understanding of quantum effects.

But why to study particles? This question is both easy and hard to answer. The easy answer is to say that it is same question as: Why to study physics? The answer to that is, from my point of view, to better the chances for the survival of mankind. The other way of answering is by referring to the various uses of the information gained by particle physics. One of the main uses of this information is astrophysics and cosmology in general. They are using this information for finding out how the universe came to existence and how it is evolving. But for those who want to have immediate results one could quote Michael Faraday, one of the main characters in finding out the laws of electromagnetism: "Why, sir, there is every possibility that you will soon be able to tax it! (to PM William Gladstone, on the usefulness of electricity)".

1.1 History of particle physics

1.1.1 From Greek philosophy to radiochemistry

This section is based on book by Hudson[3]. One of the first written thoughts about the building blocks of matter are from the ancient Greeks. First were Thales of Miletos (circa 585 BC), Anaximander (c. 555 BC), Anaximenes (c. 535 BC) and Heraclitus (c. 500 BC) who formulated the theory of four substances: fire, air, water and earth. After them came Democritus of Abdera who formulated the idea of atom (atomon, indivisible in Greek). But unfortunately Aristotle was against the atomic theory and as

he was considered as the highest authority of the sciences for 2000 years, the progress on this field was very slow.

Until the 18th century the world was considered to be made of the classical substances and quintessence (known also as the ether). After the fire was deleted from the list of the elements circa 1785 and French chemists published a list of the undiviable elements, in the spirit of the Carl Linné's scientific nomenclature of plants, the scientific world was ready for the John Dalton's theory of atoms.

Next step towards the modern understanding was the periodical system of elements by Mendeleev. He managed to organize the known elements in a periodical table and even predict the existence of some, at that time, unknown elements as well as their properties. The last step in understanding matter from the point of chemistry was the discovery of radioactivity and the beginning of radiochemistry, which could also be considered particle physics. The radioactivity gave a glance to the atom and showed us that the atom is not really nondivisible.

1.1.2 From early particle physics to quarks

The first real elementary particle (as far as we know), the electron, was discovered in the mid-1890's and the charge-to-mass ratio was determined by J. J. Thomson[4]. He also formulated the so called "plum-pudding" model of the atom. Experiments done by Geiger and Marsden produced a lot of data about the electromagnetic structure of the atom. This data allowed Rutheford[2] to formulate a more correct theory of a positively charged pointlike nucleus and electrons outside of the nucleus.

The next step on the path to the modern understanding was the planetary model of the atom by Bohr[5]. This model is actually unstable in the classical sense and not "correct" in our current knowledge. But it is still useful in simple problems[1]. This was soon followed by the formulation of quantum mechanics by many great minds. One of the greatest theoretical predictions was made by Dirac when he predicted the antimatter, in the form of positrons[6]. The year 1932 was a year of experimental findings, both the positron and the neutron were found that year. After finding the neutron, Heisenberg was able to present a proton-neutron nuclear model, which gave an explanation for the isotopes.

The following decades and the discovery of more and more "elementary" particles gave a need for the same kind of work in physics as was

[1]Like Newtonian mechanics is not correct in the view of quantum mechanics and relativity, but is still useful in simple problems

done by Mendeleev in chemistry. This work was made independently by Gell-Mann and Yuval Ne'man. Later, in 1964, Gell-Mann predicted subparticles which could be the real elementary particles behind the properties of particles found so far, and called these particles "quarks"[7]. The quark model of nucleon, seen on the figure (1), is quite similar to the "plum-pudding model" of Thomson.

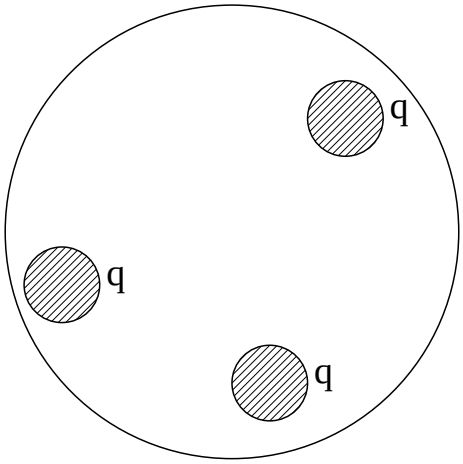

Figure 1: A nucleon made of quarks

1.1.3 Partons, QCD and modern experiments

It took more than 10 years for the idea of quarks to be universally accepted in the world of physics. Before the acceptance there were a lot of confusing results in the experiments which could not be explained by current theories. To explain these results Feynman[8] (1969) introduced and refined the theory of partons and their bindings. This theory was expanded by Bjorken and Paschos[9]. It was the birth of the parton model.

The 1970's was the decade of QCD, quantum chromodynamics, the field theory of quarks and gluons, which bind the quarks to make particles. There was no single person behind the QCD, but a large group of physicists. Modern QCD can sometimes predict the results in experiments with so great an accuracy that the error in measurements is greater than errors in the prediction. But there are still some open problems in QCD and it is still being improved.

Now as the LHC[2] at CERN is about to start operating, experimentalist are busy finalizing the construction of experiments in it, and many of those include the charm-quark to which I'll return later. In the USA, the Tevatron of Fermilab and the RHIC[3] at Brookhaven are, among other things, hunting for the Higgs boson and the reason for the mass.

1.2 Charming D-mesons

The particles which consist of the c- or $\bar{c}$-quark and a lighter (anti)quark are collectively called the D-mesons. They were first experimentally discovered in 1976 in the Stanford Linear Accelerator Center[10]. The SLAC also pioneered the study of the properties of D-mesons, for example the mass and decay channel studies. Unfortunately, the c-quark studies were largely left aside because of other, more interesting studies.

At the turn of the century charm physics got back into the spotlight of particle physics as a tool to understand the standard model, and for advancing beyond the standard model. There are a lot of open questions in charm physics including the branching ratios of D decays, $D^0 - \overline{D^0}$ mixing, CP violation. These questions are discussed in detail in the works of Alex Smith[11] and Harry J. Lipkin[12] (decays).

In this light it is important to give some predictions of the D-meson production according to the parton model.

[2]Large Hardron Collider
[3]Relativistic Heavy Ion Collider

2 Parton model, part 1 - basics and going in

While proposing the parton model[8] Feynman didn't mention quarks at all. Bjorken and Paschos[9] brought the quarks and a quark-antiquark background to the parton model, figure (2).

The first part of the parton model essentially says that baryons and mesons are build of smaller particles which are bound to each other, but can be considered to be non-interacting when the collision is considered in the infinite momentum frame. When colliding at large enough energies the model predicts probabilities for which an inner particle, or as we call them a parton, is hit, and what the momentum fraction of the parton is of particle's total momentum. Now we know that the partons are gluons, quarks and antiquarks.

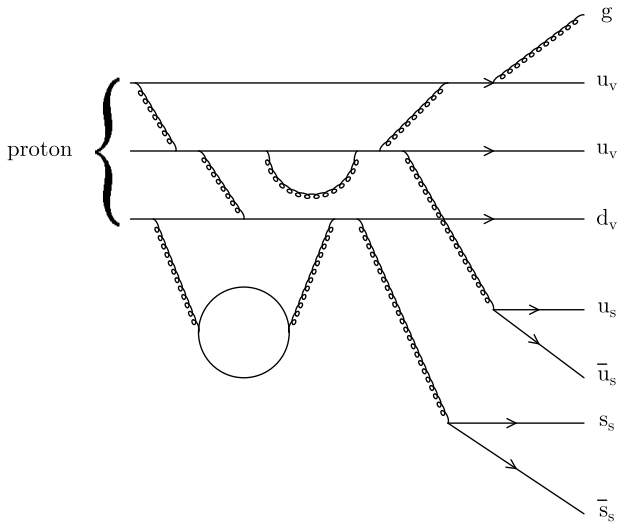

Figure 2: Proton with (anti)quark-gluon background

The second part of the parton model is the factorization of the cross-section. Discussion about what the cross-section is follows in next section. But now we just cite that the cross-section σ for the hadron-hadron collision in a naive parton model is build of parton distribution functions (see section 2.3) $f_{i/h}$ for finding the parton i in the hadron h, partonic cross-section $\hat{\sigma}(i+j \to k+\text{anything})$ (section 3.1) for reaction between partons i and j, and fragmentation functions D_k^h (section 3.2) for "finding" a hadron

h from fragmentation products of parton k:

$$\sigma(h1+h2 \to h3+\text{anything}) = \sum f_{i/h1} \otimes f_{j/h2} \otimes \hat{\sigma}(ij \to k+\text{anything}) \otimes D_k^{h3} \quad (1)$$

The kinematics (table 1) of the collision is based on the distribution of the momentum to the different partons in the baryon with the parton i having momentum xp and rest of the partons having total momentum $(1-x)p$.

	Baryon	Parton
Energy	E	xE
Momentum	p_l	xp_l
	$p_t = 0$	$p_t = 0$
Mass	M	$m = \sqrt{x^2E^2 - x^2p_l^2} = xM$

Table 1: Parton model kinematics

Usually partons with the possible exception of heavy quarks are treated massless, but this can lead to problems in some cases.

2.1 High energy collisions and cross-sections

In high energy physics collisions are not quite the same as collisions in everyday life. A more correct definition of a collision is an interaction between particles. From interactions considered here[4] all except electromagnetic scattering, equation (2), are short range interactions. Usually the probability of target and beam particle to interact is very small, but we have a very large number of both particles in a small volume, and this allows us to have some interactions which we are looking for. The cross-section σ_i describes the probability of interaction i. Mathematically it describes the area, in which a point-like particle has to hit in order to produce the wanted interaction.

On colliding beam experiments the luminosity L of the collider is defined by particles and the geometry of the beams. The average interaction rate is simply $L\sigma_i$ for the interaction i. A differential cross-section $\frac{d\sigma}{d\Omega}$ is the cross-section for a specific out going particle to scatter into the solid angle $d\Omega$.

As each interaction has its own σ which also depends on interaction energies, it gives us information of interacting particles. When we have

[4]We neglect the gravitation here

knowledge about structure of the particles we can predict new σ's for unmeasured interactions.

One of the simplest collision cross-sections is the coulombic electron scattering from a target particle or a charge distribution as illustrated in figure (3). The differential cross-section is:

$$\frac{d\sigma}{d\Omega} = \left(\frac{d\sigma}{d\Omega}\right)_{point} |F(q)|^2 \tag{2}$$

Here $F(q)$ is the electromagnetic form factor of the target, more specifically it is the Fourier transform of the charge distribution of the target. But in modern high energy colliders the energies are high enough to study quark and gluon distributions inside of nucleons and the equation (2) is not valid as such.

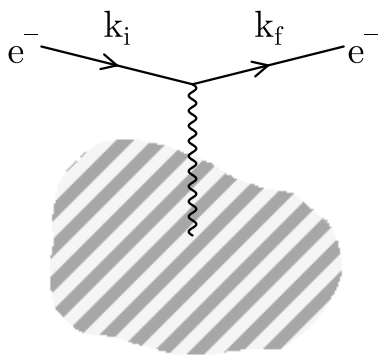

Figure 3: Measuring charge distribution of a charge cloud

The cross-section for scattering from a point charge is:

$$\left(\frac{d\sigma}{d\Omega}\right)_{point} = \frac{(Z\alpha)^2 E^2}{4k^2 \sin^4 \frac{\theta}{2}} \left(1 - v^2 \sin^2 \frac{\theta}{2}\right) \tag{3}$$

where $k = |\mathbf{k_i}| = |\mathbf{k_f}|$ and $\mathbf{k_{i/f}}$ are the initial and final momenta of the scattering electron, E is the energy of the electron, $v = k/E$, and θ is the scattering angle of the electron.

The differential cross-section for the scattering of lepton from lepton is

$$d\sigma \sim L^{\mu\nu} L_{\mu\nu} \tag{4}$$

where $L^{\mu\nu}$ is the leptonic tensor which includes among other information spin dependence. And in the case of lepton scattering from a nucleon the differential cross-section is

$$d\sigma \sim L_{\mu\nu} W^{\mu\nu} \tag{5}$$

where $W^{\mu\nu}$ is the electromagnetic hadronic tensor.

2.2 The Structure of the nucleon

Since the days of Dirac and Pauli physicists have been probing the structures of nucleons. Photoproduction and electroproduction[13] have long been important tools in it, and are still being used, see [14] and [15]. Using these and various other methods including bombarding the target with other particles and measuring the momentum and other properties of in- and outgoing particles one can get quite a lot of information of the target, see figure (3).

We still can't describe a nucleon without resorting to measured quantities. Nevertheless during last century our knowledge has increased remarkably. From the 40's the measured quantity i the electromagnetic form factor for each mucleon, like in equation (2). Before the parton model, and energies resolving quarks, the measured quantities were components of the hadronic tensor $W^{\mu\nu}$, equation (11).

In QED[5] the differential cross-section $AB \to CD$ is:

$$\left.\frac{d\sigma}{d\Omega}\right|_{cm} = \frac{1}{64\pi^2 s}\frac{p_f}{p_i}|\mathfrak{M}|^2 \tag{6}$$

In the equation p_i is the initial momentum of scattering particles, p_f the final momentum, s is Mandelstam's s-variable (see A.1) which is in the center-of-mass frame just $(E_A + E_B)^2$ and the $\mathfrak{M}$ is the invariant amplitude of the scattering. To simplify calculations we can usually average $|\mathfrak{M}|^2$ over all possible spin configurations. For example in the case of electron-electron scattering (Moller scattering):

$$-i\mathfrak{M} = (ie\bar{u}_C\gamma^\mu u_A)\left(\frac{-ig_{\mu\nu}}{q^2}\right)(ie\bar{u}_D\gamma^\nu u_B) - (ie\bar{u}_D\gamma^\mu u_A)\left(\frac{-ig_{\mu\nu}}{q^2}\right)(ie\bar{u}_C\gamma^\nu u_B) \tag{7}$$

[5]Quantum ElectroDynamics

and the averaging is done by:

$$|\mathfrak{M}|^2 \to \overline{|\mathfrak{M}|^2} \equiv \frac{1}{(2s_A+1)(2s_B+1)} \sum_{spin} |\mathfrak{M}|^2 \tag{8}$$

where s_A and s_B are the spins of the incoming particles.

It is convenient to separate summations by defining the leptonic tensor $L_i^{\mu\nu}$.

$$\overline{|\mathfrak{M}|^2} = \frac{e^4}{q^4} L_i^{\mu\nu} L^j_{\mu\nu} \tag{9}$$

where

$$L_i^{\mu\nu} = 2(k'^{\mu}k^{\nu} + k'^{\nu}k^{\mu} - (k' \cdot k - m_i^2)g^{\mu\nu}) \tag{10}$$

This leptonic tensor can be calculated through perturbation theory, unlike the hadronic tensor.

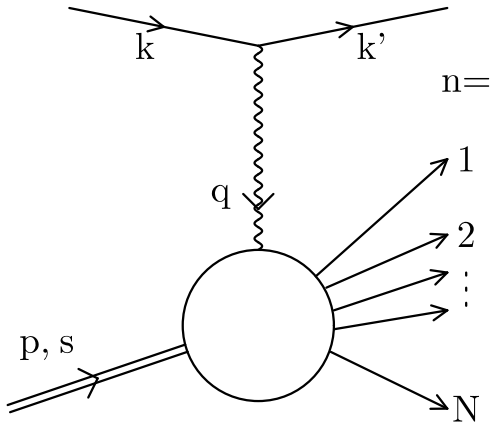

Figure 4: ep->eX process

In figure (4) we show a basic inelastic process of an electron breaking up a proton to N different objects ($ep \to eX$) with an invariant mass of $W^2 = (p+q)^2$. In this kind of processes the hadronic tensor $W^{\mu\nu}$ is used for calculations.

$$W^{\mu\nu} = -W_1 g^{\mu\nu} + \frac{W_2}{M^2} p^{\mu}p^{\nu} + \frac{W_4}{M^2} q^{\mu}q^{\nu} + \frac{W_5}{M^2}(p^{\mu}q^{\nu} + q^{\mu}p^{\nu}) \tag{11}$$

Note that this equation lacks the term W_3, which is a parity violating term and only comes into effect in neutrino-hadron cross-sections. The hadronic tensor (11) is reducible in the $ep \to eX$ process into two independent elements $W_1(q^2, \zeta)$ and $W_2(q^2, \zeta)$, where $\zeta \equiv \frac{p \cdot q}{M}$, M being the mass of the nucleon. Some details of the reduction through current conservation are found in Halzen & Martin[16] pages 180-181.

$$W^{\mu\nu} = W_1 \left(-g^{\mu\nu} + \frac{q^\mu q^\nu}{q^2} \right) + W_2 \frac{q}{M} \left(p^\mu - \frac{p \cdot q}{q^2} q^\mu \right) \left(p^\nu - \frac{p \cdot q}{q^2} q^\nu \right) \tag{12}$$

The differential cross-section is:

$$\left. \frac{d\sigma}{dE' d\Omega} \right|_{lab} = \frac{\alpha^2}{4E^2 \sin^4 \frac{\theta}{2}} \left\{ W_2(q^2, \zeta) \cos^2 \frac{\theta}{2} + 2W_1(q^2, \zeta) \sin^2 \frac{\theta}{2} \right\} \tag{13}$$

where E and E' are the initial and final electron energies. One can see some definite relationship with equation (3 in the denominator.

Bjorken scaling[17] comes into effect when the momentum transfer q^2 is large enough for a direct interaction of the photon and a quark inside the nucleon. Bjorken scaling simply states that:

$$MW_1(Q^2, \zeta) \to F_1(\omega) \tag{14}$$

and

$$\nu W_2(Q^2, \zeta) \to F_2(\omega) \tag{15}$$

where,

$$Q^2 \equiv -q^2 \quad \text{and } \omega = \frac{2M\zeta}{Q^2}$$

Nowadays we take quarks for granted, but it took about a decade and lots of measurements[18] from the proposals by Gell-Mann[7] and Zweig[19] in the year 1964 to be generally accepted. Gell-Mann himself thought quarks to be mainly a mathematical tool for some calculations and not real particles [6]

2.3 Parton distribution functions

In parton model the form factors $F_i(\omega)$, equations (14-15), can be expressed in terms of parton distribution functions (PDF) $f_i(x)$. As we consider the

[6] "It is fun to speculate about the way quarks would behave if they were physical particles of finite mass (instead of purely mathematical entities as they would be in the limit of infinite mass)." [7].

electromagnetic interaction the sum has the charge of the parton, e_i, in it. Because the gluons have charge of zero, they do not interact in a lowest order case. When energies are large enough, partons can be considered free Dirac particles and that brings the δ-function into the equation. $f_i(x)$ tells us how the momentum is distributed between the partons:

$$F_2(\omega) = \sum_i \int dx e_i^2 f_i(x) x \delta(x - \frac{1}{\omega}) \tag{16}$$

and

$$F_1(\omega) = \frac{\omega}{2} F_2(\omega). \tag{17}$$

With the δ-function the variable ω can be replaced with $x = \frac{1}{\omega} = \frac{Q^2}{2M\nu}$:

$$2xF_1(x) = F_2(x) = \sum_i e_i^2 x f_i(x). \tag{18}$$

You can find a derivation of this equation of electromagnetic interaction in many books[7].

Each parton species has its own f_i, where the index i defines different quarks, antiquarks and gluons. From quantum numbers and other restrictions we can derive some restrictions on these PDF's, for example the number of valence quarks and isospin symmetry for values of up and down quarks in proton and neutron. The restrictions from conservation laws are usually called sum rules [20].

The usual notation for PDF's is $f_{i/h}(x)$, where i is the parton and h is the hadron. So in this notation and with isospin symmetry:

$$f_{u/p}(x) = f_{d/n}(x) \tag{19}$$

The differential cross-section for the $ep \to eX$ process can be written as

$$M\nu_{max} \frac{d\sigma}{dxdy} = \frac{2\pi\alpha^2}{x^2y^2} \left\{ xy^2 F_1 + \left[(1-y) - \frac{Mxy}{2\nu_{max}} \right] F_2 \right\} \tag{20}$$

where

$$y = \frac{p \cdot q}{p \cdot k} \underset{lab}{=} \frac{\nu}{E}$$

and

$$\nu_{max} \underset{lab}{=} E$$

There are multiple different parametrizations of measured PDF's. The PDFLIB[8] has circa 150 parametrizations available to the user[21].

[7] For example Halzen & Martin [16] pages 188-194

[8] Part of CERNLIB software package

2.3.1 PDF evolution

In the original naive parton model Bjorken scaling (equations 14 and 15) removes the Q^2 dependence from the PDF's. However, QCD predicts the radiation of gluons from the high energy quarks. This behavior brings Q^2 dependence back to the equations given by the Altarelli-Parisi evolution equations [22]. A comparison of experimental values to evolution calculation is found in figure (5). These results are one of the evidences of the correctness of QCD. A more detailed discussion of the matter is out of the scope of this work. Also out of the scope are nuclear PDF's (for example [23] and [24]), which are calculated for the heavier nuclei like Pb.

As an example of leading order (LO) evolved parton distribution functions we will use CTEQ5L distributions[25] from the PDFLIB[21]. We plotted a gluon distribution at evolution scale $Q = 5GeV$ from it to figure 6.

Another modern distribution function is for example EHKQS[26]. It is not present in version 8.04 of PDFLIB, but is available through internet[9]. The comparison between CTEQ5L and EHKQS can be found on the EHKQS paper[26]. Around the $Q = 5$ GeV area the differences in gluon distribution are neglible on small x between CTEQ5L and EHKQS.

[9] http://www.urhic.phys.jyu.fi/EHKQS/EHKQS.html

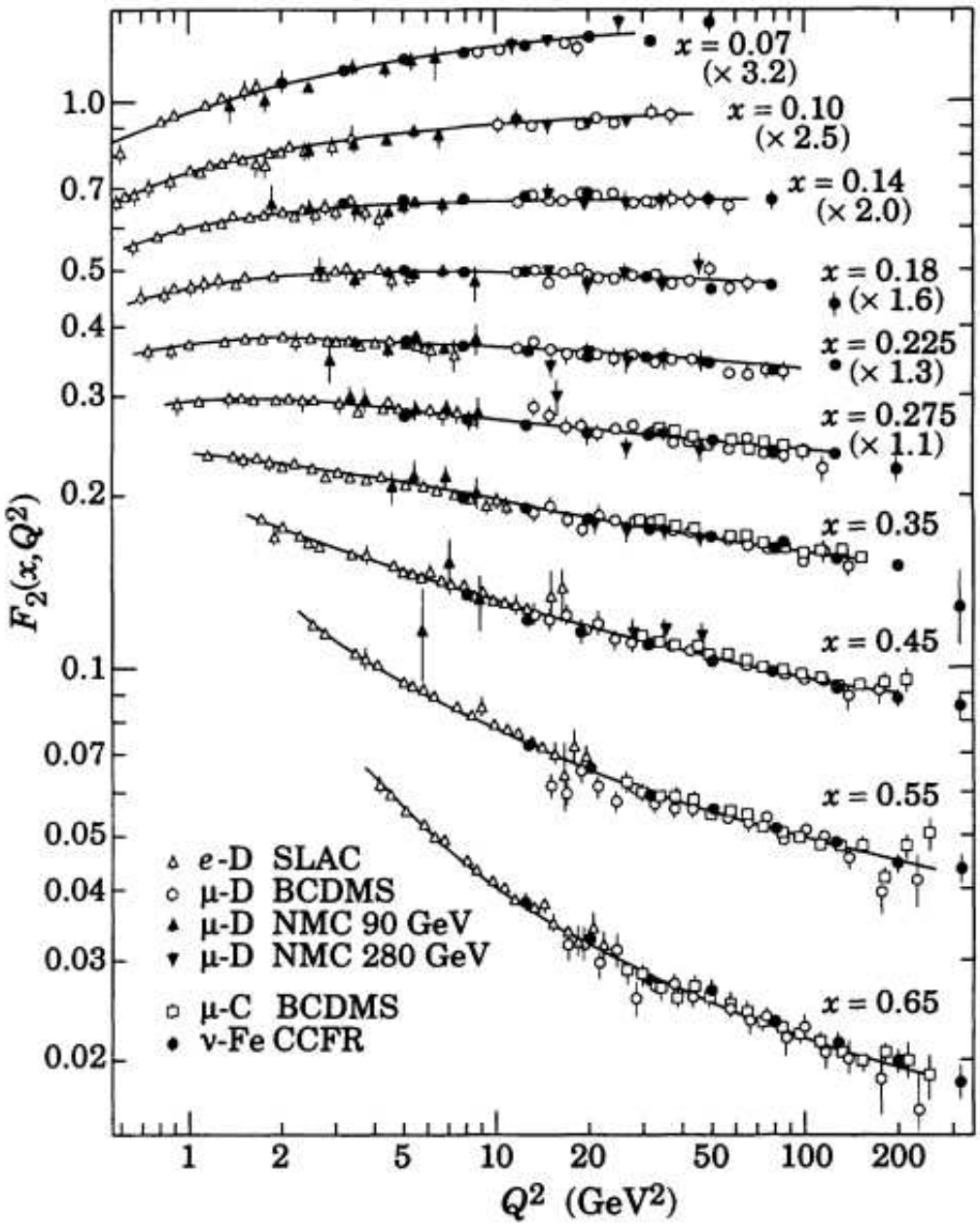

Figure 5: Q^2 dependence of F_2 in deep inelastic electron-proton scattering. The curves show the variation of F_2 for fixed x and the comparison of this variation to a model evolved with the Altarelli-Parisi theory. The data were compiled by M. Virchaux and R. Voss for the Particle Data Group, Phys. Rev. D50, 1173 (1994), Fig. 32.2. There one can also find complete references.

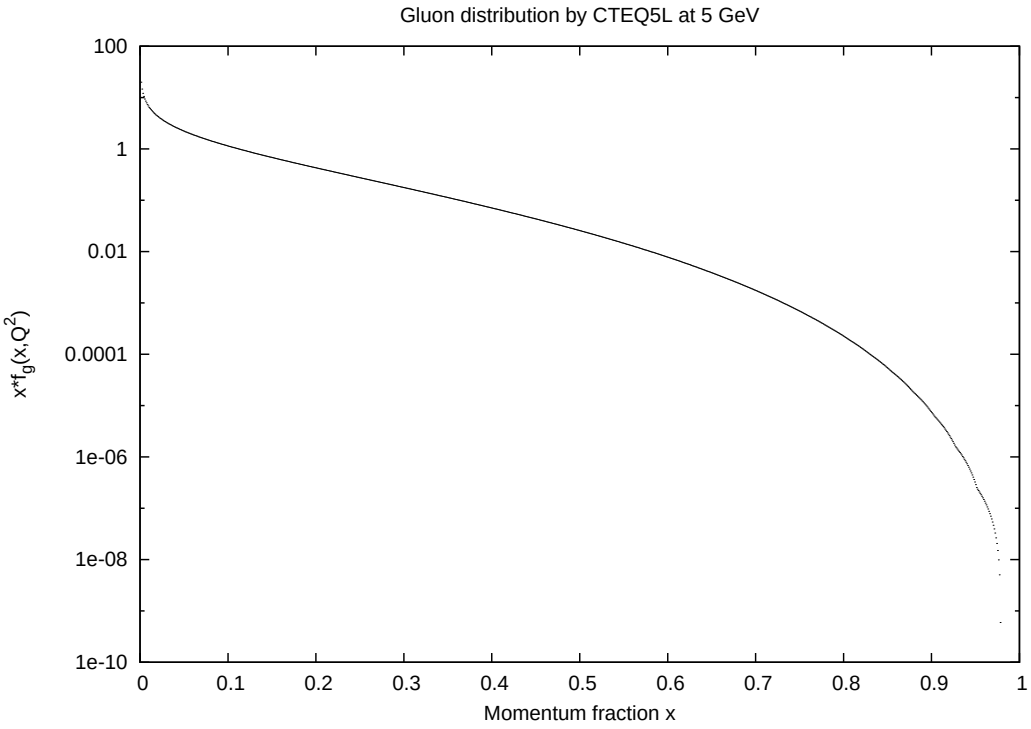

Figure 6: Gluon distribution according to CTEQ5L parametrisation[25] plotted at $Q = 5\,\mathrm{GeV}$

3 Parton model, part 2

3.1 Parton - parton cross section

In the previous chapter we talked about methods for studying partons inside a nucleon using lepton nucleon scattering. When two high energy nucleons collide in such a way that a pair of partons from colliding nucleons undergo a collision with a large momentum transfer, such collisions can be described in terms of the parton distribution functions and parton-parton cross-sections. All these cross-sections can be calculated directly from the field theories of Quantum Chromodynamics and Quantum Electrodynamics like in ref. [27]. The calculation would start from the Lagrangian of the particles. The field theory will lead to the S-matrix, which includes the non-interactive identity matrix $\mathbb{I}$ and the rest is defined as the transition matrix T.

$$S = \mathbb{I} + iT \tag{21}$$

From now on we will only consider $2 \to 2$ collisions and will be working with momentum eigenstates. The T includes an explicit momentum conservation in the form of a δ-function:

$$\begin{aligned} &iT((p_1, s_1) + (p_2, s_2) \to (p_3, s_3) + (p_4, s_4)) = (2\pi)^4 \delta^4(p_1 + p_2 - p_3 - p_4) \\ &\times \mathfrak{M}((p_1, s_1) + (p_2, s_2) \to (p_3, s_3) + (p_4, s_4)). \end{aligned} \tag{22}$$

The $\mathfrak{M}$ is scattering amplitude, from which we can calculate quantum mechanical cross sections:

$$\begin{aligned} &d\sigma((p_1, s_1) + (p_2, s_2) \to (p_3, s_3) + (p_4, s_4)) = \frac{1}{4\sqrt{(p_1 \cdot p_2)^2 - m_1^2 m_2^2}} dPS \\ &\times |\mathfrak{M}((p_1, s_1) + (p_2, s_2) \to (p_3, s_3) + (p_4, s_4))|^2. \end{aligned} \tag{23}$$

This is integrated over the phase space:

$$dPS = \prod_i \left(\frac{d^3 p_i}{2\omega_i (2\pi)^3} \right) N_i (2\pi)^4 \delta^4 \left(p_1 + p_2 - p_3 - p_4 \right), \tag{24}$$

where $\omega_i = \sqrt{p_i^2 + m_i^2}$ and N_i is the normalization for each type of particles with its value depending on the normalization of wavefunctions.

From these equations (23 and 24) we get:

$$\frac{d\sigma}{dt} = \frac{1}{16\pi s^2} |\mathfrak{M}|^2, \tag{25}$$

where s and t are Mandelstam variables, see A.1.

3.1.1 Feynman diagrams

$\mathfrak{M}$ is usually calculated with help of Feynman diagrams. Feynman rules give each propagator, vertex function and external lines a mathematical representation from which diagrams can be calculated. This calculation includes imposing momentum conservation, integration over momentum in loops and division by a symmetry factor. An external line is a line that doesn't have any more interactions in it and it represents initial and final states. A connected diagram means that there is no direct external line from incoming particle to outgoing particle or each incoming particle experiences an interaction with another particle. An amputated diagram means that self-interactions (for example quark emitting and then absorbing the same gluon) on the external line are taken out of the calculation. For the process with specified initial and final particles:

$$i\mathfrak{M} = \text{sum of all connected, amputated diagrams.} \tag{26}$$

Each graph describes one of the infinite possible ways of the interaction to happen. These graphs are organized by their order, which is the number of interaction vertices in it. The higher the order, the more unlikely it is for the interaction to happen through that path. Usually there is no need for considering other than few lowest orders of the graphs.

The mathematical representation, for parts of the graphs in the QCD, are shown in figure (7).

In our case the differential cross section is calculated from $\mathfrak{M}$ by squaring it and averaging it in terms of incoming color and spin, though sometimes the spins are calculated explicitly.

3.1.2 Examples of cross-section calculations

The differential cross section for gluon+gluon to quark+antiquark, figure (8), will be calculated here as an example, while others will be taken directly from literature (for example [28]). This cross section is used as an example also in an appendix of the paper by Schneider, Greiner and Soff [29], but here some of the calculations will be shown in greater detail and particles are considered as massless.

First we shall draw the three Feynman graphs of lowest order of the interaction, these are in figure (8). The graphs are describing different channels of the interaction, from bottom to top: s-, t-, and u-channels. The channels are named after Mandelstam variables A.1.

In the s-channel graph we have shown also the momentum, polarization and color charge of the gluons and the momentum and spin of

External lines

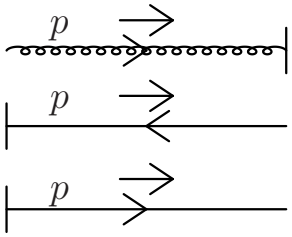

$\epsilon_\mu(p)$

$v^s(p)$

$\bar{u}^s(p)$

Propagators

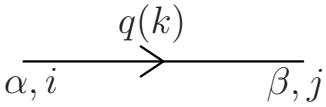

$i\frac{\delta_{ij}[\not{k}+m]}{k^2-m^2}$

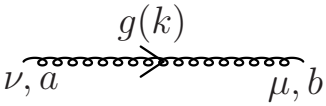

$\frac{-i\delta_{ab}g_{\mu\nu}}{k^2}$

Vertices

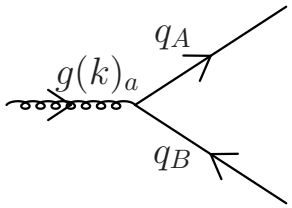

$ig\gamma^\mu t^a$

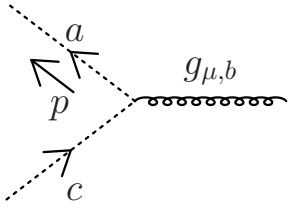

$-gf^{abc}p^\mu$

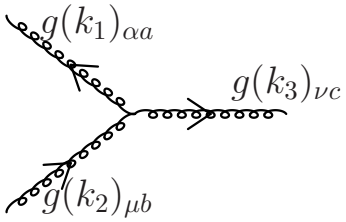

$gf^{abc}[(k_1-k_2)^\nu g^{\alpha\mu}+$
$(k_2+k_3)^\alpha g^{\nu\mu}+(k_3-k_1)^\mu g^{\alpha\nu}]$

Figure 7: Feynman rules used in this work

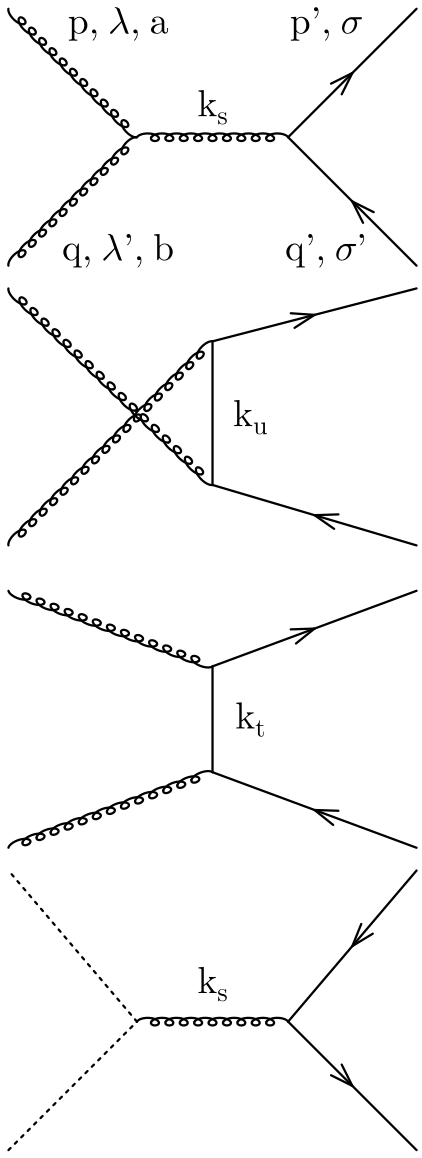

Figure 8: Feynman graphs of the reaction $g + g \to q + \overline{q}$

(anti)quarks. Using these momenta the Mandelstam variables are, in the massless limit:

$$s = (p+q)^2 = (p'+q')^2 = 2p\cdot q = 2p'\cdot q' = k_s^2 \tag{27}$$

$$t = (p'-p)^2 = (q'-q)^2 = -2p\cdot p' = -2q\cdot q' = k_t^2 \tag{28}$$

$$u = (q'-p)^2 = (p'-q)^2 = -2q'\cdot p = -2q\cdot p' = k_u^2 \tag{29}$$

$$s+t+u = 0 \tag{30}$$

The total $\mathfrak{M}$ is in this ($gg \to q\bar{q}$) case :

$$\begin{aligned}\mathfrak{M} &= \varepsilon_\lambda^\mu \varepsilon_{\lambda'}^\nu \overline{u}_\sigma(p') \left\{ \frac{-ig_s^2}{t} t^a t^b \gamma_\mu \not{k}_t \gamma_\nu + \frac{ig_s^2}{u} t^a t^b \gamma_\mu \not{k}_u \gamma_\nu + \frac{g_s^2}{s} t^c f_{cab} \right. \\ &\quad \left. \cdot\gamma^\eta \left[(k_s+p)_\mu g_{\eta\nu} + (q-p)_\eta g_{\nu\mu} - (q+k_s)_\nu g_{\mu\eta} \right] \right\} v_{\sigma'}(q') \\ &= \mathfrak{M}_t + \mathfrak{M}_u + \mathfrak{M}_s \end{aligned} \tag{31}$$

By using these definitions

$$|\mathfrak{M}|^2 = |\mathfrak{M}_t|^2 + |\mathfrak{M}_u|^2 + |\mathfrak{M}_s|^2 + 2Re\{\mathfrak{M}_t\mathfrak{M}_u^* + \mathfrak{M}_u\mathfrak{M}_s^* + \mathfrak{M}_s\mathfrak{M}_t^*\} \tag{32}$$

As you can see from equation (31), we are using the Feynman gauge for the gluon propagator. When this is combined with the gluon polarization sum used in equation (36), which includes nonphysical polarizations, there appears so-called ghost contribution. This ghost contribution has to be removed from equation (32):

$$|\mathfrak{M}|^2 = |\mathfrak{M}_t|^2 + |\mathfrak{M}_u|^2 + |\mathfrak{M}_s|^2 + 2Re\{\mathfrak{M}_t\mathfrak{M}_u^* + \mathfrak{M}_u\mathfrak{M}_s^* + \mathfrak{M}_s\mathfrak{M}_t^*\} - |\mathfrak{M}_G|^2. \tag{33}$$

The calculation of the ghost cross-section is similar to all other partial cross-section calculations.

First we shall calculate unpolarized and color averaged $|\mathfrak{M}_t|^2$.

$$\begin{aligned}\overline{|\mathfrak{M}_t|^2} &= \frac{1}{4}\frac{1}{8^2} \sum_{\substack{\sigma\sigma'\lambda\lambda' \\ color}} \mathfrak{M}_t \mathfrak{M}_t^* \\ &= \frac{1}{4\cdot 8^2} \sum_{\substack{\sigma\sigma'\lambda\lambda' \\ color}} \varepsilon_\lambda^\mu \varepsilon_{\lambda'}^\nu \overline{u}_\sigma(p') \frac{-ig_s^2}{t} t^a t^b \gamma_\mu \not{k}_t \gamma_\nu v_{\sigma'}(q') \\ &\quad \cdot \left(\varepsilon_\lambda^\eta \varepsilon_{\lambda'}^\delta \overline{u}_\sigma(p') \frac{-ig_s^2}{t} t^a t^b \gamma_\eta \not{k}_t \gamma_\delta v_{\sigma'}(q') \right)^* \end{aligned} \tag{34}$$

By using equation (128) in appendix B.2 on page 45 we have

$$\overline{|\mathfrak{M}_t|^2} = \frac{g_s^4}{4\cdot 8^2 t^2} \sum_{\substack{\sigma\sigma'\lambda\lambda' \\ \text{color}}} \varepsilon_\lambda^\mu \varepsilon_{\lambda'}^\nu \, \overline{u}_\sigma(p') \, t^a t^b \gamma_\mu \not{k}_t \gamma_\nu v_{\sigma'}(q') \\ \overline{v}_{\sigma'}(q') \, \gamma_\delta \not{k}_t \gamma_\eta u_\sigma(p') t^b t^a \varepsilon_{\lambda'}^{\delta *} \varepsilon_\lambda^{\eta *} \tag{35}$$

And then moving polarization vectors next to each other and t^i's as well

$$\overline{|\mathfrak{M}_t|^2} = \frac{g_s^4}{4\cdot 8^2 t^2} \sum_{\substack{\sigma\sigma'\lambda\lambda' \\ \text{colors}}} \varepsilon_\lambda^\mu \underbrace{\varepsilon_{\lambda'}^\nu \varepsilon_{\lambda'}^{\delta *}}_{-g^{\nu\delta}} \varepsilon_\lambda^{\eta *} t^a t^b t^b t^a \\ \overline{u}_\sigma(p')\gamma_\mu \not{k}_t \gamma_\nu v_{\sigma'}(q') \overline{v}_{\sigma'}(q') \gamma_\delta \not{k}_t \gamma_\eta u_\sigma(p') \tag{36}$$

Summation over λ's, applying $-g^{\iota\kappa}$'s from polarization sums and summation of colors gives:

$$\overline{|\mathfrak{M}_t|^2} = \frac{g_s^4}{4\cdot 8^2 t^2} \sum_{\sigma\sigma'} \mathrm{tr}(t^a t^b t^b t^a) \overline{u}_\sigma(p') \gamma_\mu \not{k}_t \gamma_\nu v_{\sigma'}(q') \overline{v}_{\sigma'}(q') \gamma^\nu \not{k}_t \gamma^\mu u_\sigma(p') \tag{37}$$

Then by writing explicitly down the spinor indices we can move $\overline{u}_\sigma(p')$ and sum over σ and σ' to get $\not{q}'$ and $\not{p}'$. Writing down spinor indices also means taking the trace of the part of the equation.

$$\overline{|\mathfrak{M}_t|^2} = \frac{g_s^4}{4\cdot 8^2 t^2} \mathrm{tr}(t^a t^b t^b t^a) \mathrm{tr}(\not{p}' \gamma_\mu \not{k}_t \gamma_\nu \not{q}' \gamma^\nu \not{k}_t \gamma^\mu) \tag{38}$$

This trace is calculated in appendix B.4 at equation (134) on page 46 and the result is:

$$\overline{|\mathfrak{M}_t|^2} = \frac{g_s^4}{16 t^2} \mathrm{tr}(t^a t^b t^b t^a)[2(p'\cdot k_t)(q'\cdot k_t) - (k_t\cdot k_t)(p'\cdot q')] \tag{39}$$

By using equations (27-30) we get.

$$\begin{aligned}
\overline{|\mathfrak{M}_t|^2} &= \frac{g_s^4}{16 t^2} \mathrm{tr}(t^a t^b t^b t^a) \left[2(p'(p'-p))(q'(q-q')) - t\frac{1}{2}s \right] && (40)\\
&= \frac{g_s^4}{16 t^2} \mathrm{tr}(t^a t^b t^b t^a) \left[2(\underbrace{p'p'}_{0} - p'p)(q'q - \underbrace{q'q'}_{0}) + t\frac{1}{2}(t+u) \right] && (41)\\
&= \frac{g_s^4}{16 t^2} \mathrm{tr}(t^a t^b t^b t^a) \left[-\frac{1}{2}t^2 + \frac{1}{2}t^2 + \frac{1}{2}tu \right] && (42)\\
&= \frac{g_s^4}{32 t} \mathrm{tr}(t^a t^b t^b t^a) u && (43)
\end{aligned}$$

Next using appendix B.5 on page 46:

$$\overline{|\mathfrak{M}_t|^2} = \frac{g_s^4}{32t}\frac{16}{3}u = \frac{1}{6}g_s^4\frac{u^2}{ut} \tag{44}$$

All other calculations are more or less similar to this and we shall just note their results using the shorthand notation $\mathfrak{M}_{ut} = 2\,\mathrm{Re}\,\mathfrak{M}_u\mathfrak{M}_t^*$ here in equations (45-51).

$$\begin{aligned}
\overline{|\mathfrak{M}_t|^2} &= \frac{1}{6}g_s^4\frac{u^2}{ut} && (45)\\
\overline{|\mathfrak{M}_u|^2} &= \frac{1}{6}g_s^4\frac{t^2}{ut} && (46)\\
\overline{|\mathfrak{M}_s|^2} &= -\frac{3}{8}g_s^4\frac{2u^2+2t^2+\frac{3}{2}ut}{s^2} && (47)\\
\overline{|\mathfrak{M}_{ut}|^2} &= 0 && (48)\\
\overline{|\mathfrak{M}_{us}|^2} &= -\frac{3}{8}g_s^4\frac{u^2}{us} && (49)\\
\overline{|\mathfrak{M}_{st}|^2} &= -\frac{3}{8}g_s^4\frac{t^2}{ts} && (50)\\
\overline{|\mathfrak{M}_G|^2} &= \frac{3}{8}g_s^4\frac{\frac{1}{2}tu}{s^2} && (51)
\end{aligned}$$

The final result is:

$$\begin{aligned}
\overline{|\mathfrak{M}|^2} &= g_s^4\Big(\frac{1}{6}\frac{t^2+u^2}{tu} - \frac{3}{8}\frac{2u^2+2t^2+\frac{3}{2}ut+us+ts+\frac{1}{2}ut}{s^2}\Big)\\
\overline{|\mathfrak{M}|^2} &= g_s^4\Big(\frac{1}{6}\frac{t^2+u^2}{tu} - \frac{3}{8}\frac{u^2+t^2}{s^2}\Big). && (52)
\end{aligned}$$

Combining this result with (25) and defining $\alpha_s = g_s^2/4\pi$ we get:

$$\frac{d\overline{\sigma}}{dt} = \frac{\pi\alpha_s^2}{s^2}\Big(\frac{1}{6}\frac{t^2+u^2}{tu} - \frac{3}{8}\frac{u^2+t^2}{s^2}\Big) \tag{53}$$

Similar calculations can be done to other partonic cross-sections.

Combining equations (1) and (53) we now have the differential cross-section for the production of massless quark-antiquark pair through gluon-gluon channel in proton-proton collision. We will use this massless approximation to calculate the c quark production:

$$\frac{d^3\overline{\sigma}}{dx_1dx_2dt}(p+p\to c+\bar{c}) = f_{g/p}(x_1)\times f_{g/p}(x_2)\frac{\pi\alpha_s^2}{s^2}\Big(\frac{1}{6}\frac{t^2+u^2}{tu} - \frac{3}{8}\frac{u^2+t^2}{s^2}\Big) \tag{54}$$

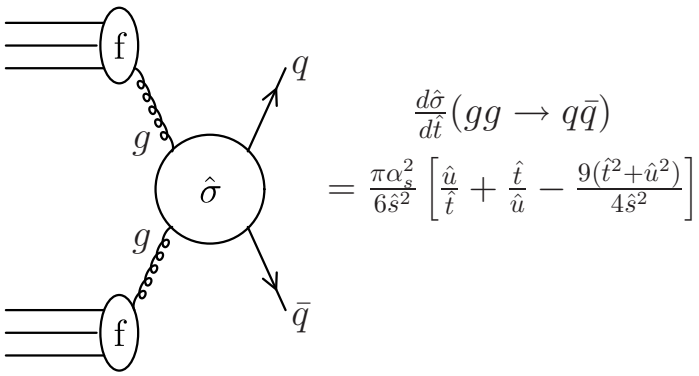

Figure 9: $gg \to q_i\overline{q}_i$ scattering

The relationships between x_i and Mandelstam variables are to be discussed in section 4

3.2 Fragmentation and jet formation

We shall take color confinement as an experimentally confirmed hypothesis. This confiment states that no single (anti)quark or gluon exists as a free particle, because they are color charged objects, as the total color charge of a free particle has to be zero.

This confinement is behind the creation of hadrons from the scattered partons. There are multiple different parametrizations of measured data for this parton fragmentation to hadrons and few phenomenological schemes. These are discussed in some detail in ref. [30].

In the same way as the PDF describes the probability to find a quark inside a hadron, the fragmentation functions $D_i^h(z, Q^2)$ describe the probability to find the hadron h from the quark i at the momentum fraction z of the total momentum of the quark at the energy scale Q^2. We shall use the delta function fragmentation for c-quarks: $D_c^{h(c)}(z) = \delta(1-z)$. Here the $h(c)$ means a hadron with a c-quark. This scheme approximates a scenario where all of the momentum of the quark goes to the particle with the c-quark (D-meson usually). It would be better justified on low p_t case, where one can assume that one of the light spectator quarks[10] is "captured" by the hadron formed in fragmentation[31], but it still gives a reasonably accurate D-meson distribution for our use and effectively means that we can use equation (54) without any modification.

[10]the quark which didn't participate in the main interaction

With this fragmentation model there is no difference in production of charged and neutral D-mesons, so we can approximate that half of produced mesons are charged and rest are neutral. This approximation is confirmed and production rates of excited states are from reference[32]:

$$N(D^0) : N(D^+) : N(D^{*0}) : N(D^{*+}) = 1 : 1 : 3 : 3 \tag{55}$$

This triple production of excited states arises from available spin states (ground state is singlet: J=0 and exciteted state is triplet: J=3). These rates leads to conclusion that $1/8$th of produced c-quarks fragment to D^0-mesons and same $1/8$th to D^+-mesons.

The jets are formed around the fragmented initial quarks and their decay products. There are many definitions for the hadron jet and jet dynamics is a very important part for reconstructing an underlying event from measured hadrons. For example the book of Ellis, Stirling and Webber[28] uses three chapters for the jet properties (including the formation of a jet).

3.2.1 D-meson decay

The D-mesons are unstable particles and decay through weak interaction, except in the case of the excited states D^*, which decay also through electromagnetic interaction, a thorough discussion of D^* is out of the scope of this work. We shall only make a few notes of the decay of the non-excited states of D and cite results collected by Particle Data Group[30]. In the weak decay the theory of quark flavor mixing, described by the CKM matrix[33] and [34], is responsible for the decay. There are two Cabibbo allowed decays of the c-quark: $c \to s + l^+ + \nu_l$ ($l = e, \mu$) and $c \to s + u + \bar{d}$. Cabibbo suppressed decays are not as likely as the Cabibbo allowed decays. These allowed decay modes mean that D-mesons decay mainly to K-mesons (kaon) and leptons or pions. The presence of Cabibbo suppressed decays allows other decay modes in addition. Most notable of these for the charged D-mesons are pionic modes (no K-mesons) and modes with two K-mesons, for uncharged D-mesons there are also modes with three K-mesons. If the produced K-meson is in its excited state it may decay further in the time-frame of the reaction, but K-mesons can be considered stable particles when compared to D-mesons. The mean life τ for the D^+ is $1040 \pm 7 \times 10^{-15}$s and for the D^0 $410.1 \pm 1.5 \times 10^{-15}$s.

We are interested in detectable D-mesons and for it the length which it travels before decay is important. In order to calculate it we start with exponential decay law:

$$-\frac{dP(l)}{dl} = \lambda P(l) \tag{56}$$

$$P(l) = Ce^{-\lambda l} \tag{57}$$

$$1 = \int_0^\infty dl\ C\ e^{-\lambda l} \rightarrow C = \lambda \tag{58}$$

$$P(l) = \lambda e^{-\lambda l} \tag{59}$$

The λ is $1/\tau_l$, where τ_l is the mean length of flight before decay and it is calculated from:

$$\tau_l = \tau \cdot \gamma \cdot v, \tag{60}$$

where τ is the mean life of the D-meson, γ is the Lorentz factor and v is the speed of the D-meson. These lead to:

$$\tau_l = \tau \cdot \frac{p}{m}. \tag{61}$$

When using GeVs for units of momenta and mass, we need to add the speed of light to the equation to get result in SI units:

$$\tau_l = \tau \cdot c \cdot \frac{p[GeV]}{m[GeV]}. \tag{62}$$

So in conclusion we have:

$$\frac{dP(l)}{dl} = \frac{m[GeV]}{\tau \cdot c \cdot p[GeV]} e^{-\frac{l \cdot m[GeV]}{\tau \cdot c \cdot p[GeV]}}. \tag{63}$$

4 Kinematics of a $2 \to 2$ parton process

The process is shown in figure (10).

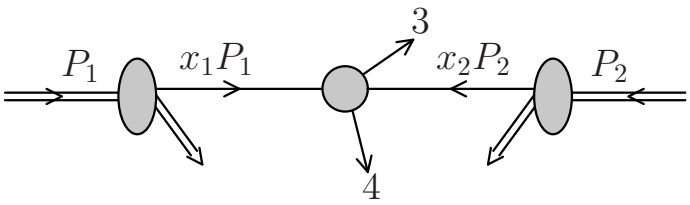

Figure 10: $2 \to 2$ partonic scattering

We shall work now in the hadron-hadron center of mass frame in the high-energy limit and thus ignoring the hadron masses. This implies the following momenta for the hadrons:

$$P_1 = (E, 0, 0, E) \tag{64}$$

and

$$P_2 = (E, 0, 0, -E). \tag{65}$$

Here we shall use the following convention for Mandelstam variables: if they are without a hat (s, t, u) they are for the hadrons and with a hat$(\hat{s}, \hat{t}, \hat{u})$ they are for the partons. From the definition of s (equation 116 on A.1):

$$s = 4E^2 \tag{66}$$

The 4-momentum of the parton-parton collision, q, is defined in the following way:

$$q = x_1P_1 + x_2P_2 = \big((x_1 + x_2)E, 0, 0, (x_1 - x_2)E\big), \tag{67}$$

where $x_{1,2}$ are the momentum fractions of the colliding partons. The invariant square, also known as the square of the invariant mass, of this vector is:

$$q^2 = M^2 = x_1x_2s = \hat{s} \tag{68}$$

Also by definition:

$$q^0 = M \cosh Y, \tag{69}$$

where the Y is the center of the mass of colliding partons.

From these we get

$$\begin{aligned} q^0 = M \cosh Y &= (x_1 + x_2)E & (70)\\ \cosh Y &= (x_1 + x_2)\frac{E}{M} & (71)\\ &= \frac{x_1 + x_2}{2\sqrt{x_1 x_2}} = \frac{1}{2}\Big(\sqrt{\frac{x_1}{x_2}} + \sqrt{\frac{x_2}{x_1}}\Big), & (72) \end{aligned}$$

which implies from the definition of cosh:

$$\exp Y = \sqrt{\frac{x_1}{x_2}}. \tag{73}$$

From this and equation (68) we get:

$$x_1 = \frac{M}{\sqrt{s}} e^Y \tag{74}$$

and

$$x_2 = \frac{M}{\sqrt{s}} e^{-Y}. \tag{75}$$

Now we are ready to move to parton variables with still assuming massless particles. The cross-section is from equation (54), with slight modifications to notations:

$$\frac{d^3\sigma}{dx_1 dx_2 d\hat{t}}(hh- > 3 + 4 + X) = f_1(x_1) f_2(x_2) \frac{d\hat{\sigma}}{d\hat{t}}, \tag{76}$$

where f_i are the distribution functions first mentioned in (18).

The (longitudinal) rapidity y_i for particle i can be defined through the energy of the particle E_i or through the longitudinal momentum p_{li}, with the help of transverse momenta p_t. As the total transverse momentum is zero before the collision, it will be zero also after the collision. So its value is the same, but the direction is opposite for both outgoing particles (3 and 4).

$$E_i = p_t \cosh y_i \tag{77}$$

$$p_{li} = p_t \sinh y_i \tag{78}$$

In on the center of momentum frame for colliding partons, the total energy is $\sqrt{\hat{s}}$. This same frame is also the center of momentum frame for scattered partons 3 and 4. Variables in this frame will be marked with subscript *. In the CM frame the rapidities are $y_{3*} = -y_{4*} = y_*$.

From the additivity of rapidity we get:

$$y_* = \frac{1}{2}(y_3 - y_4) \tag{79}$$

and

$$Y = \frac{1}{2}(y_3 + y_4). \tag{80}$$

The transverse momentum is by definition:

$$p_{t*} = \frac{1}{2}\sqrt{\hat{s}}\sin\theta_*, \tag{81}$$

where θ_* is the scattering angle in the center-of-mass frame.

From this, and the energy of the particle and from equation (77) we get:

$$\begin{aligned} E_{3*} = \frac{1}{2}\sqrt{\hat{s}} &= p_3\cosh y_* && (82)\\ &= \frac{1}{2}\sqrt{\hat{s}}\sin\theta_*\cosh y_* && (83)\\ \frac{1}{\sin\theta_*} &= \cosh y_* && (84) \end{aligned}$$

The longitudinal momentum is:

$$p_{l*} = \frac{1}{2}\sqrt{\hat{s}}\cos\theta_*. \tag{85}$$

From this and equations (81, 78 and 84):

$$\begin{aligned} p_{l*} = \frac{1}{2}\sqrt{\hat{s}}\cos\theta_* &= p_t\sinh y_* && (86)\\ &= \frac{1}{2}\sqrt{\hat{s}}\sin\theta_*\sinh y_* && (87)\\ \frac{\sinh y_*}{\cosh y_*} &= \cos\theta_* && (88)\\ \tanh y_* &= \cos\theta_* && (89) \end{aligned}$$

From appendix A.1 and these results we get:

$$\hat{s} = 4p_t^2\cosh^2 y_* \tag{90}$$

and

$$\begin{aligned}\hat{t} &= -2p_t^2 \cosh^2 y_* (1 - \tanh y_*) && (91)\\ &= -2p_t^2 \cosh y_* (\cosh y_* - \sinh y_*) && (92)\\ &= -2p_t^2 \cosh y_* e^{-y_*}. && (93)\end{aligned}$$

From equations (68, 74, 75 and 90) we get:

$$x_1 = \frac{2p_t}{\sqrt{s}} \cosh y_* e^{Y} \tag{94}$$

and

$$x_2 = \frac{2p_t}{\sqrt{s}} \cosh y_* e^{-Y}. \tag{95}$$

From all these we can translate the cross section equation (76) to measurable variables (meaning rapidities and p_t). This happens through the Jacobian:

$$\frac{\partial(x_1, x_2, \hat{t})}{\partial(y_3, y_4, p_t)} = \frac{8p_t^3}{s} \cosh^2 y_* = \frac{2p_t \hat{s}}{s} = x_1 x_2 2p_t. \tag{96}$$

In the last part of the equation we used this fact. Now the cross section is:

$$\frac{d^3\sigma}{dy_3 dy_4 dp_t} = x_1 f_1(x_1) x_2 f_2(x_2) 2p_t \frac{d\hat{\sigma}}{d\hat{t}}. \tag{97}$$

5 Experimental particle physics

We will only discuss high energy physics (HEP) here, as D-meson production happens only at high energies. Some neutrino physics experiments could be examples of low energy particle physics. The energy scale of particle physics continues rising from the first particle physics experiments. One of the reasons for more energetic experimental facilities is the higher energy available which means that heavier particles can be produced and in greater numbers. Other reasons include for example the study of parton distribution functions in greater detail at lower values of x, equation (18). In the 70's accelerators had sufficient energy for D-meson production but statistics were quite low for them.

An event is a term used in physics which means a detected collision. There are mainly two ways to get events to study. From nature we get for example cosmic rays. The more controlled way of producing them is to accelerate particle beams to high energies and let them collide with a target. New particles are created from the energy in the collision between the beam and the target.

5.1 Accelerators and colliders

In a e^+/e^- beam (or in the future μ^+/μ^- beams[35]) the energy of colliding particles is known with great precision as the beam particles don't have internal structure, but like the parton model dictates, in a hadronic beam the energy of a particle is divided unequally between the constituents of the hadron. This distribution of energy between partons reduces the available energy in a collision.

The first particle accelerators were just high voltage generators which produced high velocity electrons.

Generally the two most important factors for accelerators and colliders in HEP are the the available energy for the reaction and the reaction rate. The energy available in colliders is the total energy of two colliding beams and thus usually higher than the energy of fixed target accelerators.

The reaction rate in a collider is:

$$R = \sigma L, \tag{98}$$

where L is luminosity. The luminosity describes how many interactions can possibly happen in a particle bunch crossing.

One of the mathematical definitions [36] for luminosity in bunch-type beams is:

$$L = N_1 N_2 f W_x W_y, \tag{99}$$

where N_1 and N_2 are the numbers of particles in bunches 1 and 2, f is the bunch crossing frequency, and:

$$W_x = \frac{\int D_{1x}(x) D_{2x}(x) dx}{\int D_{1x}(x) dx \int D_{2x}(x) dx}$$

$$W_y = \frac{\int D_{1y}(y) D_{2y}(y) dy}{\int D_{1y}(y) dy \int D_{2y}(y) dy}.$$

Indices y and x are horizontal and vertical directions, while subindices 1 and 2 refer to colliding bunches. Functions D are the independent particle densities in their directions. The integrals extend over the full beam size.

A simpler and more easily understandable definition is:

$$L = f n \frac{N_1 N_2}{A}, \tag{100}$$

where f is the revolution frequency, n is the number of bunches in either beam around the ring, N is the number of particles in a bunch and A is the cross-sectional area of the beams (assuming total overlap on collision).

For a fixed target accelerator the reaction rate is:

$$R = \sigma \frac{N \delta_t l}{t}, \tag{101}$$

where δ_t is is the number density of target particles, l is the thickness of the target and t is the time between bunches.

Usually the reaction rate for fixed targets is higher than in colliders.

The characteristics of previously and currently operated machines are collected in the table (2).

5.2 LHC - Large Hadron Collider

When the LHC is finished in November 2007 it will be the most energetic collider ever built and it shall remain so for some time as the USA has cancelled their Superconducting Super Collider project. We can still be quite sure that some day there will be an even more powerful collider and there are multiple designs for what to come, for example CLIC[37] or a muon collider[35].

As the name indicates, it will collide hadrons, not leptons and this has both beneficial and adverse effects on the project. The radiation energy

Name	type	beam energy(GeV)	major find
CERN PS	p synchrotron	28	
BNL AGS	p synchrotron	32	Charm, CP-violation,ν_μ
SLAC	e^- linac	25-50	Charm quark
SLC	e^-e^+ collider	50+50	
LEP1	e^-e^+ collider	50+50	
LEP2	e^-e^+ collider	100+100	number of neutrino flavors
SPS	p synchrotron	450	
Sp$\overline{\text{p}}$S	p$\overline{\text{p}}$ collider	310 +310	
HERA	ep collider	30e+820p	
Tevatron I	p$\overline{\text{p}}$ collider	900+900	top quark
Tevatron II	p$\overline{\text{p}}$ collider	980+980	
RHIC	Au^{79+} collider	100/u+100/u	
	p^+ collider	250+250	
	Cu^{29+} collider	100/u+100/u	

Table 2: Previously and currently operated machines

losses are smaller for heavier hadrons than for lighter leptons so the LHC can give more energy to the particles than a lepton collider. It will be also possible to run heavier ions in it, Pb+Pb-collisions have already been planned for it. The adverse effect of hadron collisions is the energy uncertainty in a collision. This uncertainty is due to the energy distribution of the partons inside hadrons, which we have already treated in the parton model section of this work.

LHC shall be discussed only briefly here and more details are found in ref.[38]-[42]. LHC is part of the chain of CERN accelerators of protons, and the ions which are injected to it have been accelerated in smaller machines before injection as shown in figure (11). The figure also shows us the positions of different experimental stations along the LHC ring.

The performance of the LHC is studied more in chapters 2 and 21 of ref.[39] and for maximum pp luminocity in ALICE see reference [40][11], but some of the information is given here in table (3).

5.3 Detectors

Like accelerator technology, detector technology has advanced greatly during the last century, from simple scintillation detectors and photographic plates to large detectors with multiple different subdetectors. An ionizing

[11] ALICE system is not capable of handling pile-up of events in greater luminosities

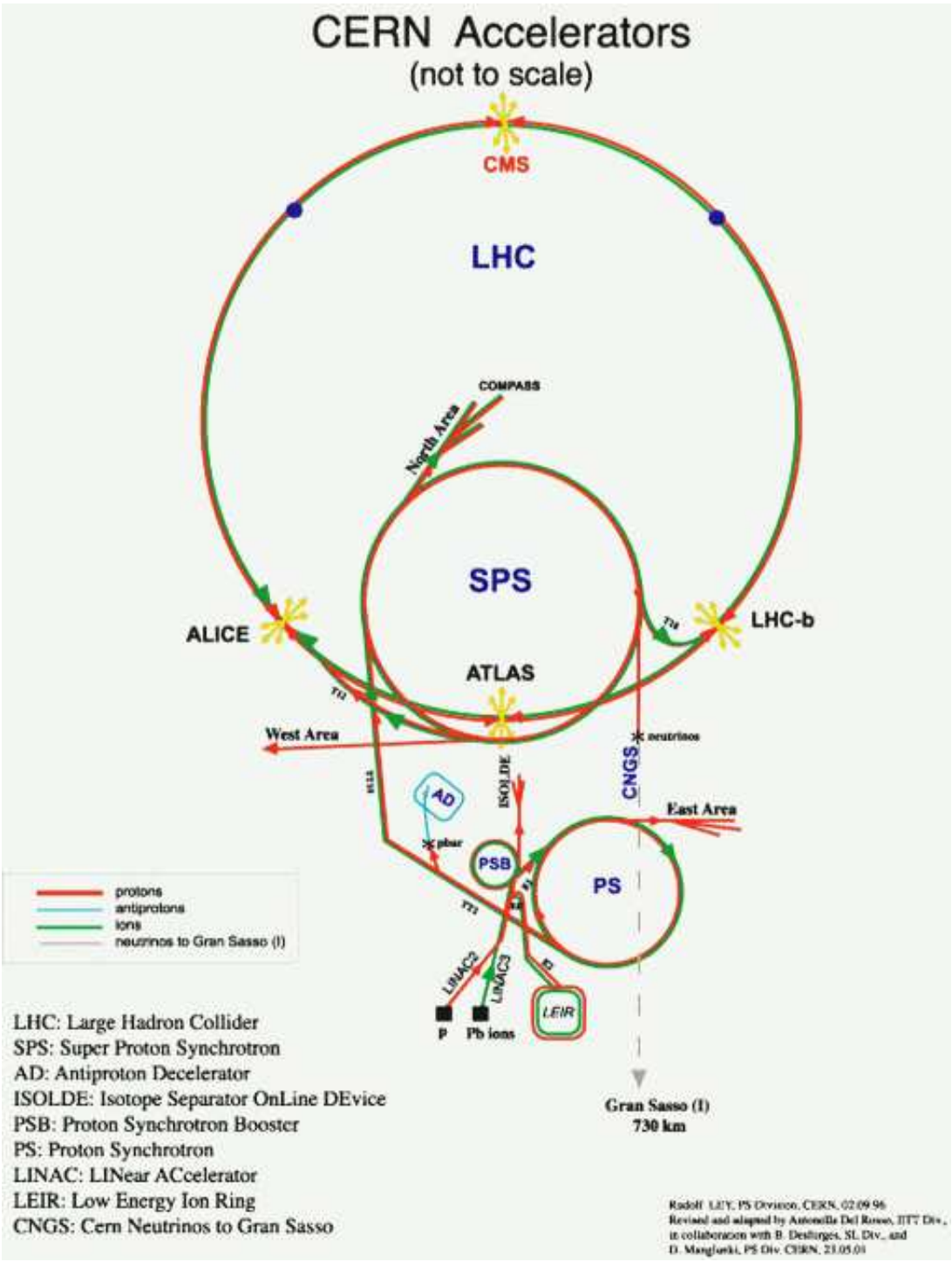

Figure 11: CERN Accelerator chain image© CERN

	Proton	$^{208}Pb^{82+}$
Energy on collision	7000 GeV	574000 GeV
Energy per nucleon	7000 GeV	2760 GeV
Number of particles per bunch	1.15×10^{11}	7×10^{7}
Number of bunches	2808	592
Peak luminosity	$1.0 \times 10^{34} \frac{1}{\mathrm{cm}^2\mathrm{s}}$	$1 \times 10^{27} \frac{1}{\mathrm{cm}^2\mathrm{s}}$
Maximum luminosity in ALICE	$3.0 \times 10^{30} \frac{1}{\mathrm{cm}^2\mathrm{s}}$	

Table 3: LHC performance

particle excites a molecule in a scintillation detector and the decay of the excitation emits a light pulse which is detected. Cloud and bubble chambers provided us possibilities to study tracks made by particles. This tracking allowed us to study the momentum(mass)/charge properties of particles as the chambers were put into a magnetic field. The passing charged particle creates a track in both types of chambers. In the cloud chamber there is supercooled water vapor and tracks of mist are condensed around ions created by passing charged particles. In the bubble chamber superheated liquid is boiled by passing ionizing particles, thus creating a track. In these chambers the tracks of particles were photographed and then analyzed.

Most modern detectors rely on ionization effects of the radiation and they then measure the produced electronic current. Semiconductor detectors can also measure the energy loss of the particle in the detector and this makes the identification of the particle easier. Drift chambers are gas filled chambers with cathode planes and anode wires to collect electrons created by passing particles.

Modern scintillation counters are usually equipped with fast electronics and operate very quickly and are therefore used in timing and triggering in experiments.

In modern experiments detectors are built of multiple separate detector elements with different functions. Multiple silicon detector elements can also be used in the observation of tracks of particles, like cloud and bubble chambers previously. The tracks are produced from the knowledge of which silicon element was hit and when. Each detector element also has its dead time, during which it is inoperative after it has detected something. This dead time produces problems as high energies of colliders produce lots of uninteresting events too and there would also be lots of unneeded data to be saved. Triggers are used to select interesting events and if a trig-

ger is not met then the whole event is discarded and the detector is ready for a more interesting event.

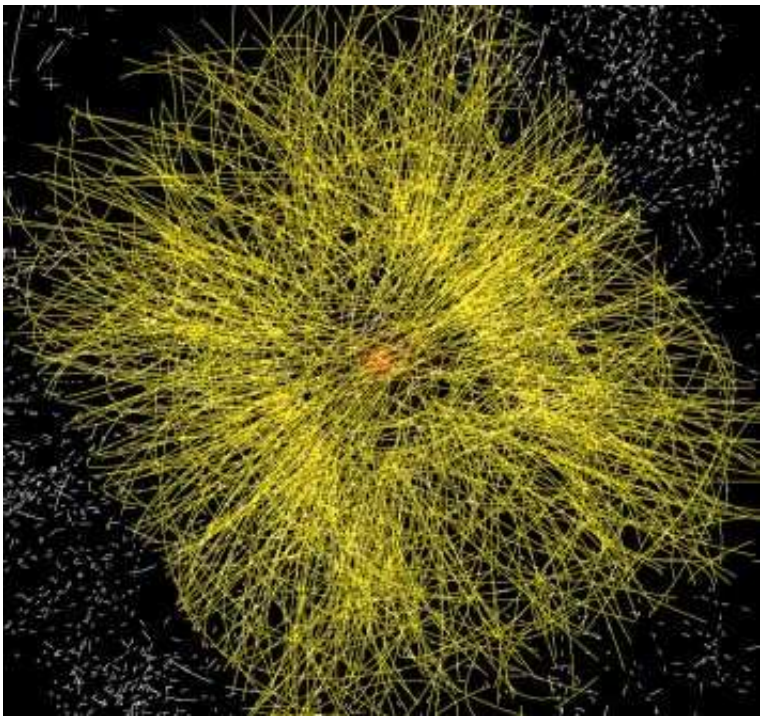

Figure 12: Tracks on a simulation of ALICE detector image© CERN

5.4 ALICE - A Large Ion Collider Experiment

ALICE (figure 13) is one of the four experiment stations in LHC which is to be operational in summer 2008. The main focus of studies in ALICE is high energy heavy ion collisions and more specifically QGP[12] and the production of open charm (D-mesons), phase transitions and hadronic matter, in non-QGP studies $\gamma\gamma$ collisions are also studied in large cross-section p+p-processes.

We start this section by giving details about the magnet and then we will continue describing the detector elements from inside out, leaving triggers out.

The ALICE main magnet[43] is taken from the previous L3 experiment from LEP[13]. It is octagonally shaped and produces a solenoid field, with

[12]Quark Gluon Plasma
[13]Large Electron Positron Collider

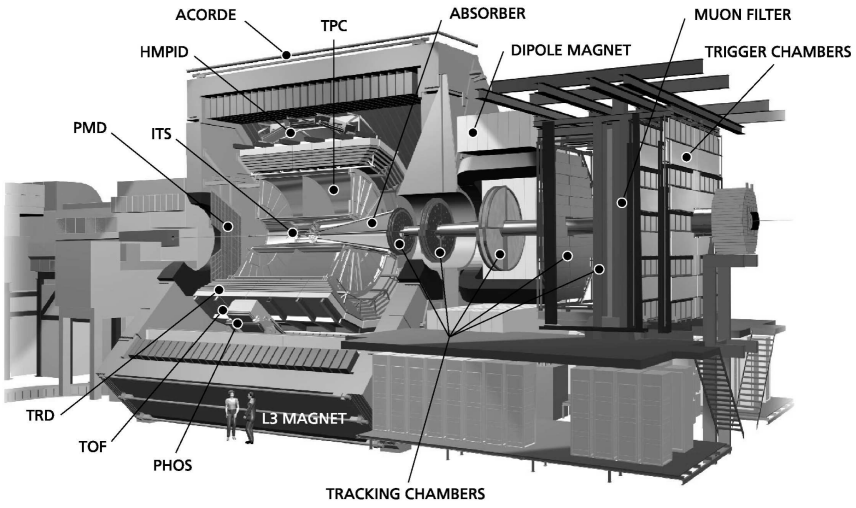

Figure 13: ALICE detector image© CERN. Note: The HMPID is in the 12 o'clock position for the sake of visibility, instead of the correct 2 o'clock position

parameters in table (4). The cooling structure of the magnet has been changed because the old system was badly corroded.

Inner radius of coil	5930 mm
Width of conductor	890 mm
Outer radius of yoke	7900 mm
Total length of coil	11900 mm
Total length of yoke	14100 mm
Total height across flats	15800 mm
Electrical power (at 0.5 T field)	4.2 MW
Central field	0.5 T
Stored energy	150 MJ
Rated current	30 kA
Current density in conductor	55.5 A/cm^2
Demineralized cooling water	150 m^3/h
Coil weight	1100t
Yoke weight	6700t

Table 4: L3 magnet parameters

The first detector from the interaction point in ALICE is the Inner Track-

ing System (ITS)[44][45][40]. It consist of 6 layers of silicon detectors, with different capabilities shown in table (5). Design considerations for ITS included a large acceptance for rapidity $|\eta| < 0.9$, dE/dx measurement capability, good spatial precision and granularity, tolerance for a large amount of radiation, high readout rate and budget restrictions. More specific tasks among others for the ITS are the localization of the primary vertex with a resolution better than 100 μm, reconstruction of the secondary vertices from decays of hyperons and D- and B-mesons, and tracking and identification of particles with momentum below 100 MeV. The first layers are expected to operate with a high track density (80 tracks/cm^2).

Layer	Type	r(cm)	±z(cm)	Area (m^2)
1	Pixel	3.9	14.1	0.07
2	Pixel	7.6	14.1	0.14
3	Drift	15.0	22.2	0.42
4	Drift	23.9	29.7	0.89
5	Strip	37.8/38.4	43.1	2.09
6	Strip	42.8/43.4	48.9	2.68

Table 5: Dimensions of ITS detectors[45]

Parameter	Silicon pixel	Silicon drift	Silicon strip
Spatial precision rϕ(μm)	12	38	20
Spatial precision z (μm)	100	28	830
Two track resolution rϕ(μm)	100	200	300
Two track resolution z(μm)	850	600	2400
Cell size (μm^2)	50×425	150×300	95×40000

Table 6: Capabilities of ITS detector elements[45]

The next detector in the outward direction is the Time-Projection Chamber (TPC)[46], which is the main tracking detector in ALICE. The time projection chamber is a drift chamber with a large drift volume[36]. The parameters of ALICE TPC are in table (7).

There are two major systems dedicated to particle identification (PID) in ALICE. The larger of them is the Time of Flight (TOF)[47] system and the second is the High Momentum Particle Identification Detector (HMPID). TOF is built of a new type of detectors, Multigap Resistive Plate Chambers[48]. On the other hand, HMPID is built of traditional Cherenkov counters. The

Pseudo-rapidity coverage	$-0.9 < \eta < 0.9$ for full radial track length $-1.5 < \eta < 1.5$ for 1/3 radial track length
Azimuthal coverage	2π
Radial position (active volume)	845 < r < 2466 mm
Radial size of vessel	780 < r < 2780 mm
Length (active volume)	5000 mm
Position resolution(σ)	
In $r\phi$	1100-800 μm (inner/outer radii)
In z	1250-1100 μm

Table 7: TPC parameters [45]

PHOton Spectrometer (PHOS) shares the status of the outmost detector with HMPID.

The simulations have given an impact parameter resolution for proton-proton collision of 60 μm in transverse coordinates and 90 μm for z-axis, on average. For Pb-Pb collisions the resolution is predicted to be better by an order of magnitude in transverse coordinates and c. 3 times better in z-axis (depending on the magnetic field of the L3 magnet)[40].

6 Simulations and analysis

One could go into philosophical discussion of the similarities of simulations and experiments, as experiments can simulate some specific situation in nature. Like the environment created in LHC collisions is quite similar to the first moments of the universe. But here we use the word simulation to describe calculations made by a computer to predict what would happen in experiments.

In simulations we can use multiple different values of parameters and get different predictions, when these predictions are compared to results from the experiments we know what parameters are the most correct ones of the used ones.

The pure calculating power of computers has risen steadily from the first computers. Now days a single home computer can have more than double the calculating power of a supercomputer from the late 1970's. Furthermore off-the-shelf computers can be easily used to create a parallel computing cluster without having to resort to buying more expensive specialized hardware. These advances have brought a lot of computing power into the hands of scientists.

Simple computing power means nothing as the computer has to be given instructions about what to do. This is done through programming and in the field of physics the standard programming language has been Fortran for decades, and the demise of it has been forecast all the time. Currently C++ is chosen to be the primary language in the LHC community, instead of FORTRAN77 and Fortran 95, nevertheless this work has been done mainly with Fortran 95, as it is more familiar to the author than C++.

As stated previously Fortran 95 is mainly used in this work, but there are some exceptions to this in the code and libraries written by others besides the author of this work. The main contributions of code are PYTHIA version 6.4.11 [50] for obtaining independent reference to my own code and PDFLIB [21] for CTEQ5L parton distribution.

6.1 D-meson detection in ALICE

As mentioned in the ALICE chapter there is a minimum length which a D-meson has to travel so that its decay is distinguishable from the main interaction vertex. The simulations done here are for giving predictions about the distribution of traveling length of the D-meson.

This is done by first calculating the momentum distribution of D-mesons $\frac{dP}{dp}(p)$ with midrapidity $y = 0$ and rapidity interval $\Delta y = 1$. Results from

the code purely for this work were verified with PYTHIA. The PYTHIA distribution was done by doing 20 000 000 simulations for single c-production and tabulated and normalized from there and presented in figure (14).

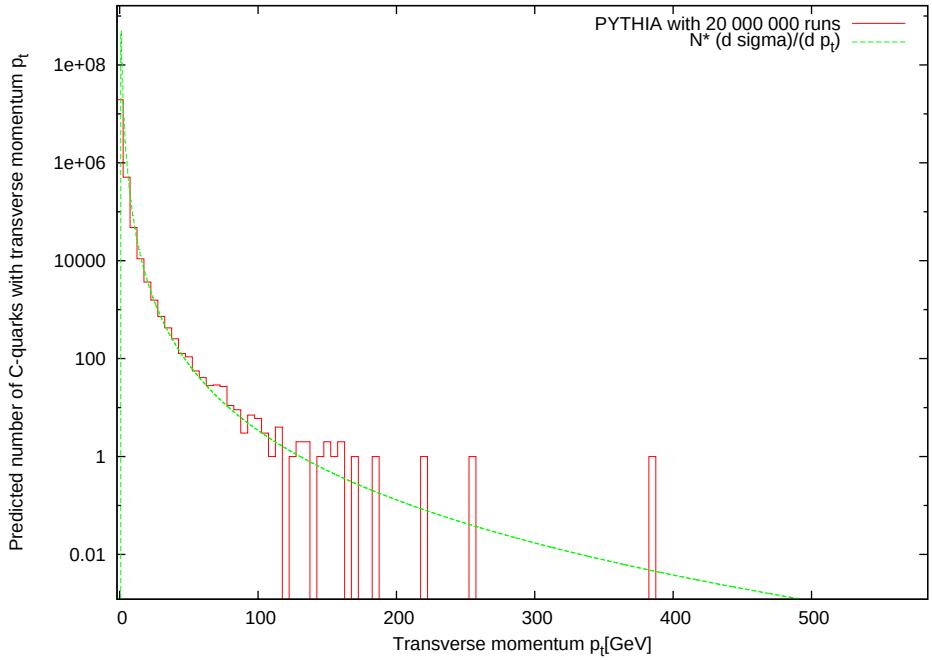

Figure 14: Comparison of p_t distribution between PYTHIA and code for this work, with integration over rapidities in both (not y=0)

$\frac{dP}{dp}(p)$ is provided in the following way:

$$\frac{dP}{dp}(p) = \frac{dP}{dp_t}\bigg|_{y_3=0}(p = p_t) = \frac{d^2\sigma}{dy_3 dp_t}\bigg|_{y_3=0}\Delta y_3 = \int dy_4 \frac{d^3\sigma}{dy_3 dy_4 dp_t}\bigg|_{y_3=0}, \tag{102}$$

where $\frac{d^3\sigma}{dy_3 dy_4 dp_t}$ is from equation (97). Notations are simplified by noting that $p = p_t$, when $y = 0$.

$$\frac{dP}{dp_t}\bigg|_{y_3=0}(p = p_t) = \frac{dP}{dp}(p) \tag{103}$$

The normalization of this distribution is also done.

$$\frac{dP}{dp}(p) = N\frac{d\sigma}{dp}(p), \tag{104}$$

where N is gotten from

$$\int_1^{7000} dp N \frac{d\sigma}{dp} = 1. \tag{105}$$

The next step to get the length of the flight distribution for D-mesons in ALICE is to combine their momentum distributions with the length of time distributions for different momenta from 63. So we have:

$$\frac{d^2P}{dpdl}(l,p) = \frac{dP}{dp}(p) \cdot \frac{dP}{dl}(l;p). \tag{106}$$

As both previous distributions have been normalized the combined distribution too is normalized. When this is integrated over p we get the pure length of the flight distribution.

$$\frac{dP}{dl}(l) = \int_1^{7000} dp \, \frac{dP}{dp}(p) \cdot \frac{dP}{dl}(l;p) \tag{107}$$

This integration has been done to both D^0 and D^+ and the resulting distributions are in figures (15) and (16)

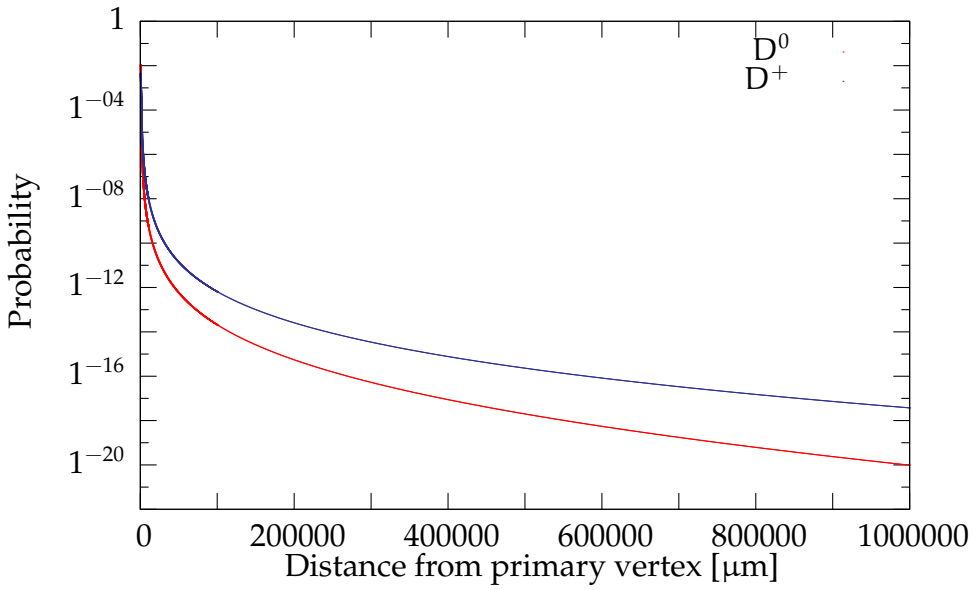

Figure 15: $\frac{dP}{dl}(l)$ distributions for D^0 and D^+ over full integration range

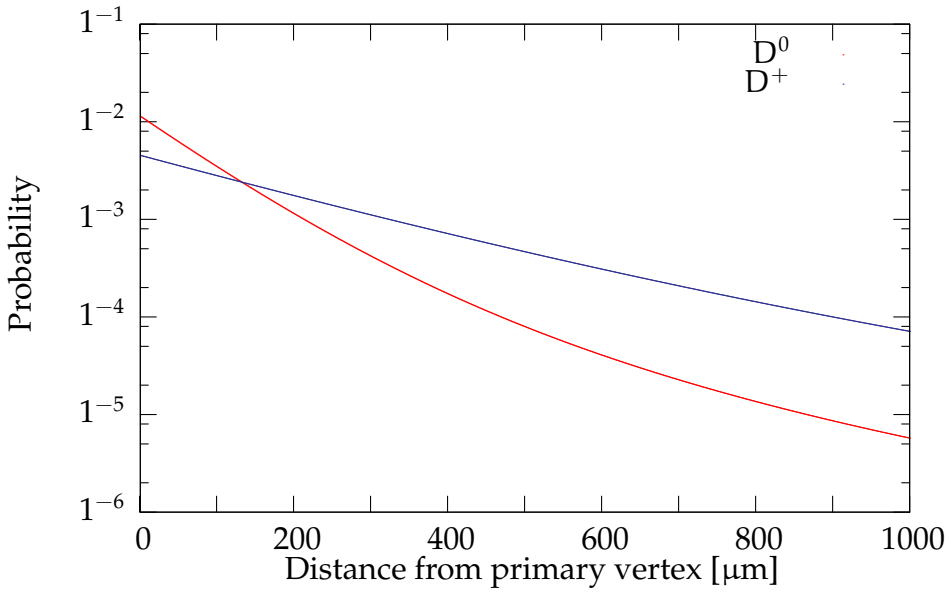

Figure 16: $\frac{dP}{dl}(l)$ distributions for D^0 and D^+ over interesting area

From these one can obtain predictions for the D-mesons in the ALICE, like probabilities for different lengths of the flight l:

$$\mu = \int_0^\infty dl\, l\, \frac{dP}{dl}(l) \tag{108}$$

$$P(l < l_i) = \int_0^{l_i} dl\, \frac{dP}{dl}(l) \tag{109}$$

$$P(l > l_i) = 1 - \int_0^{l_i} dl\, \frac{dP}{dl}(l) \tag{110}$$

$$P(l_i > l > l_j) = \int_{l_i}^{l_j} dl\, \frac{dP}{dl}(l), \tag{111}$$

and in numerical integration it is easy to obtain the lengths l at which a certain percentage of D-mesons have decayed, by ending the integration of l at the value l_i 109 when the required probability has been reached. Results from these integrations have been tabulated in table (8).

As you can see from the table almost of the D^0-mesons at zero rapidity

Distance	Probability of decay	
	D^0	D^+
l>60 μm	51%	76%
l>90 μm	37%	67%
l>120 μm	28%	59%
	Distance	
Mean length	99 μm	250 μm
Median length	63 μm	158 μm

Table 8: Decay probabilities of D-mesons in ALICE-environment

produced in proton-proton collisions do decay before they can be detected. With D^+ the situation is better as most of them do have an impact parameter larger than 60 μm. This work doesn't provide information about the ground state D-mesons coming from decay of excited states D^* as their momenta distribution is different. Another significant thing to notice is the fact that ALICE is "tuned" to Pb-Pb collisions, not to proton-proton, which has resulted compromised capabilities in p-p reaction detection.

To get an estimation for numbers of detectable events one needs to integrate the total cross-section, equation (97), and multiply it with the luminosity of LHC, from table (3). So the peak production rate for D-mesons is:

$$\begin{aligned} R &= L\sigma = L * \int dy_4 dp_t \left(\frac{d^3\sigma}{dy_3 dy_4 dp_t} \right) \Big|_{y_4=0} \Delta y_4 && (112) \\ &= L * 10 \times 10^{-27} cm^2 && (113) \\ &= 3.0 \times 10^{30} \frac{1}{cm^2 s} * 10 \times 10^{-27} cm^2 && (114) \\ &= 30000 \frac{1}{s} && (115) \end{aligned}$$

This means that LHC produces in ALICE luminosities 108 000 000 D-mesons in a run of one hour. With the previous assumptions of 1/4 of production in fragmentation being ground state D-mesons and symmetrical fragmentation of c-quark to D^+ and D^0, equation (55), half of the produced mesons are charged and rest are neutral. This results to 13 50 000 primary ground state D^0-mesons and same amount of D^+-mesons

So this combined to length of flight probabilities from table (8) we come to conclusion that there will be 6 890 000 detectable D^0 and 10 300 000 de-

tectable D^+ mesons from primary interaction in one hour of LHC operations in ALICE only. These numbers provide great statistics when compared to first experiments dedicated to D-mesons (total 48 000 events in Peruzzi et. al [51])

A 2-2 process kinematics

Many high energy physics reactions can be simplified to 2-2 collisions. We all should be familiar with different frames in kinematics, of which the center of the mass (CMS) and the laboratory (LAB) frames are the most usable ones. From here on we will use the four-vector notation, in which $P = p^\mu$, $\mu = 0, 1, 2, 3$, $p^0 = E$ and p^i normal three-dimensional momenta.

A.1 Mandelstam variables

Many calculations have a tendency to become obscure while using normal laboratory or center of mass frames. To ease some calculations there are Mandelstam variables[52] s, t and u defined by following way: P_a and P_b are incoming particles and P_1 and P_2 are outgoing particles as shown on figure (17):

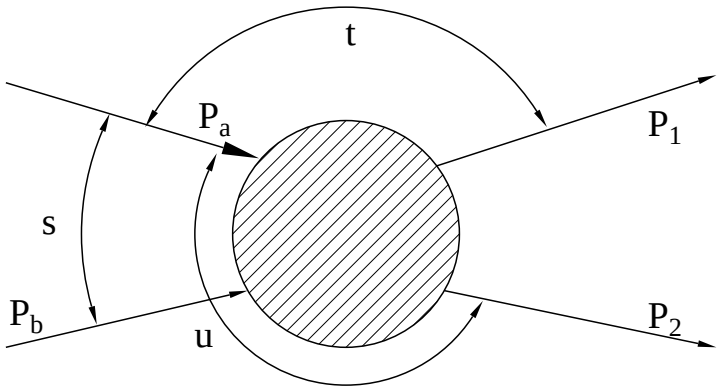

Figure 17: Mandelstam variables

$$s \equiv (P_a + P_b)^2 = (P_1 + P_2)^2 = E_{CMS}^2 \tag{116}$$

$$s = \begin{cases} (E_a^* + E_b^*)^2 = (E_1^* + E_2^*)^2 & \text{CMS} \\ \\ m_a^2 + m_b^2 + 2m_a E_a^{LAB} & \text{LAB} \end{cases}$$

Simply said, s is the energy of collision squared.

$$t \equiv (P_a - P_1)^2 = (P_b - P_2)^2 = -\frac{1}{2}s(1 - \cos\theta_{CMS}) \tag{117}$$

$$t = \begin{cases} m_a^2 + m_1^2 - 2E_a E_1 + 2|\vec{P}_a||\vec{P}_1|\cos\theta_{a1} & \text{CMS or LAB} \\ m_b^2 + m_2^2 - 2m_b E_2^{LAB} & \text{LAB} \end{cases}$$

$$u \equiv (P_a - P_2)^2 = (P_b - P_1)^2 = -\frac{1}{2}s(1 + \cos\theta_{CMS}) \tag{118}$$

$$u = \begin{cases} m_a^2 + m_2^2 - 2E_a E_2 + 2|\vec{P}_a||\vec{P}_s|\cos\theta_{a2} & \text{CMS or LAB} \\ m_b^2 + m_1^2 - 2m_b E_1^{LAB} & \text{LAB} \end{cases}$$

B Mathematical results for calculating cross-section

B.1 Usable basic information for Dirac spinors, γ and color matrices

$$u^{\dagger\dagger} = u \tag{119}$$
$$u^\dagger \gamma^0 = \overline{u} \tag{120}$$
$$\gamma^{0\dagger} = \gamma^0 \tag{121}$$
$$\gamma^{\mu\dagger} = \gamma^0 \gamma^\mu \gamma^0 \tag{122}$$
$$\gamma^0 \gamma^0 = I_4 \tag{123}$$
$$\gamma^\mu \gamma^\nu + \gamma^\nu \gamma^\mu = 2g^{\mu\nu} \tag{124}$$
$$\gamma^\mu \gamma_\mu = 4I_4 \tag{125}$$
$$t^{a\dagger} = t^a \tag{126}$$

And taking the dagger from momenta changes nothing:

$$k_t^{\rho\dagger} = k_t^\rho \tag{127}$$

B.2 Example for complex conjugation of M-matrix element

$$\begin{aligned} & \left[\varepsilon_\lambda^\mu \varepsilon_{\lambda'}^\nu \overline{u}_\sigma(p') t^a t^b \gamma_\mu \not{k}_t \gamma_\nu v_{\sigma'}(q')\right]^* \\ = \; & \left[\varepsilon_\lambda^\mu \varepsilon_{\lambda'}^\nu \overline{u}_\sigma(p') t^a t^b \gamma_\mu \not{k}_t \gamma_\nu v_{\sigma'}(q')\right]^\dagger \\ = \; & \left[\varepsilon_\lambda^\mu \varepsilon_{\lambda'}^\nu u_\sigma^\dagger(p') \gamma^0 t^a t^b \gamma_\mu \gamma_\rho k_t^\rho \gamma_\nu v_{\sigma'}(q')\right]^\dagger \\ = \; & v_{\sigma'}^\dagger(q') \gamma_\nu^\dagger k_t^{\rho\dagger} \gamma_\rho^\dagger \gamma_\mu^\dagger t^{b\dagger} t^{a\dagger} \gamma^{0\dagger} u_\sigma^{\dagger\dagger}(p') \varepsilon_{\lambda'}^{\nu\dagger} \varepsilon_\lambda^{\mu\dagger} \\ = \; & v_{\sigma'}^\dagger(q') \gamma^0 \gamma_\nu \gamma^0 k_t^\rho \gamma^0 \gamma_\rho \gamma^0 \gamma^0 \gamma_\mu \gamma^0 t^b t^a \gamma^0 u_\sigma(p') \varepsilon_{\lambda'}^{\nu*} \varepsilon_\lambda^{\mu*} \\ = \; & \overline{v}_{\sigma'}(q') \gamma_\nu \gamma^0 \gamma^0 k_t^\rho \gamma_\rho \gamma_\mu \gamma^0 \gamma^0 u_\sigma(p') t^b t^a \varepsilon_{\lambda'}^{\nu*} \varepsilon_\lambda^{\mu*} \\ = \; & \overline{v}_{\sigma'}(q') \gamma_\nu \not{k}_t \gamma_\mu u_\sigma(p') t^b t^a \varepsilon_{\lambda'}^{\nu*} \varepsilon_\lambda^{\mu*} \end{aligned} \tag{128}$$

B.3 Basic info for calculating traces

If in the trace there is an odd number of γ_μ's then it vanishes.

$$\begin{aligned} Tr(1) &= 4 && (129)\\ Tr(\not{a}\not{b}) &= 4a\cdot b && (130)\\ Tr(\not{a}\not{b}\not{c}\not{d}) &= 4[(a\cdot b)(c\cdot d)-(a\cdot c)(b\cdot d)+(a\cdot d)(b\cdot c)] && (131)\end{aligned}$$

B.4 Example for calculating trace (tt-channel case)

$$\begin{aligned} & tr(\not{q}'\gamma_\mu \not{k}_t\gamma_\nu \not{p}'\gamma^\nu \not{k}_t\gamma^\mu)\\ = \quad & tr(\not{q}'\gamma_\mu \not{k}_t\gamma_\nu\gamma_\rho p'^\rho\gamma^\nu \not{k}_t\gamma^\mu)\end{aligned}$$

Now using by equation 124

$$\begin{aligned} = \quad & tr(\not{q}'\gamma_\mu \not{k}_t(2g_{\nu\rho}-\gamma_\rho\gamma_\nu)p'^\rho\gamma^\nu \not{k}_t\gamma^\mu)\\ = \quad & tr(2\not{q}'\gamma_\mu \not{k}_t p'_\nu\gamma^\nu \not{k}_t\gamma^\mu - \not{q}'\gamma_\mu \not{k}_t\gamma_\rho p'^\rho\gamma_\nu\gamma^\nu \not{k}_t\gamma^\mu)\end{aligned}$$

By using 125 we get

$$\begin{aligned} = \quad & tr(2\not{q}'\gamma_\mu \not{k}_t\not{p}'\not{k}_t\gamma^\mu - 4\not{q}'\gamma_\mu \not{k}_t\not{p}'\not{k}_t\gamma^\mu)\\ = \quad & tr(-2\not{q}'\gamma_\mu \not{k}_t\not{p}'\not{k}_t\gamma^\mu)\end{aligned}$$

Similarly commuting γ_μ next to γ^μ on both parts of the equation we get

$$= tr(4\not{q}'\not{k}_t\not{p}'\not{k}_t) \tag{132}$$

$$= 4*4[2(q'\cdot k_t)(p'\cdot k_t)-(k_t\cdot k_t)(q'\cdot p')] \tag{133}$$

$$tr(\not{q}'\gamma_\mu \not{k}_t\gamma_\nu \not{p}'\gamma^\nu \not{k}_t\gamma^\mu) = 32(q'\cdot k_t)(p'\cdot k_t)-16(k_t\cdot k_t)(q'\cdot p') \tag{134}$$

B.5 Color traces

We call traces involving t^i or f^{abc} or their daggers color traces. Here we show how to calculate them.

$$[t^a,t^b] = i\, f^{abc}t^c \tag{135}$$

$$[t^a,t^b]^\dagger = -i\, t^{c\dagger}f^{abc\dagger} \tag{136}$$

$$[t^a,t^b] = i\, t^c f^{abc\dagger} \tag{137}$$

Here we used equation (126). With these equations all f^{abc} and their daggers can be presented with t^i-matrices.

In our traces there are only two basic combinations of t^i-matrices. A detailed derivation of the results stated here would go beyond the scope of this work and we shall just quote results from the book of Peskin and Schroeder [49].

$$t^i t^j t^i t^j = -\frac{2}{9}\mathbb{I}_3 \tag{138}$$

$$t^i t^j t^j t^i = \frac{16}{9}\mathbb{I}_3 \tag{139}$$

B.6 Calculating elements of $\overline{|\mathfrak{M}|^2}$

B.6.1 $\overline{|\mathfrak{M}_u|^2}$

$$\begin{aligned}\overline{|\mathfrak{M}_u|^2} &= \frac{1}{4}\frac{1}{8^2}\sum_{\substack{\sigma\sigma'\lambda\lambda'\\ \text{color}}} \mathfrak{M}_u \mathfrak{M}_u^* \\ &= \frac{1}{4\cdot 8^2}\sum_{\substack{\sigma\sigma'\lambda\lambda'\\ \text{color}}} \varepsilon_\lambda^\mu \varepsilon_{\lambda'}^\nu \overline{u}_\sigma(p')\frac{-ig_s^2}{u}t^a t^b \gamma_\mu \not{k}_u \gamma_\nu v_{\sigma'}(q') \\ &\quad \cdot \left(\varepsilon_\lambda^\eta \varepsilon_{\lambda'}^\delta \overline{u}_\sigma(p')\frac{-ig_s^2}{u}t^a t^b \gamma_\eta \not{k}_u \gamma_\delta v_{\sigma'}(q')\right)^*\end{aligned} \tag{140}$$

As we can see, this is identical to equation 34 (on page 19), except for $t \to u$. So we can skip a few calculations and go directly to the form of 38 and evaluate $\mathrm{tr}(t^a t^b t^b t^a) = \frac{16}{3}$.

$$\overline{|\mathfrak{M}_u|^2} = \frac{g_s^4}{4\cdot 8^2 t^2}\frac{16}{3}\mathrm{tr}(\not{p}'\gamma_\mu \not{k}_u \gamma_\nu \not{q}'\gamma^\nu \not{k}_u \gamma^\mu) \tag{141}$$

Similarly to 39-41, we get

$$\overline{|\mathfrak{M}_u|^2} = \frac{g_s^4}{3u^2}\left[2(\underbrace{p'p'}_{0} - p'q)(q'p - \underbrace{q'q'}_{0}) + u\frac{1}{2}(t+u)\right] \tag{142}$$

$$\overline{|\mathfrak{M}_u|^2} = \frac{1}{6}g_s^4\frac{t}{u} \tag{143}$$

B.6.2 $\overline{|\mathfrak{M}_s|^2}$

$$\begin{aligned}
\overline{|\mathfrak{M}_s|^2} &= \frac{1}{4}\frac{1}{8^2}\sum \mathfrak{M}_s\mathfrak{M}_s^* && (144)\\
&= \frac{1}{4}\frac{1}{8^2}\sum \varepsilon_\lambda^\mu \varepsilon_{\lambda'}^\nu \varepsilon_\lambda^{\beta *} \varepsilon_{\lambda'}^{\delta *} \frac{g_s^4}{s^2} f^{abc} t^c t^{c'} f^{abc'\dagger} \\
&\quad \cdot \bar{u}_\sigma(p')\gamma_\rho v_{\sigma'}(q')\bar{v}_{\sigma'}\gamma_\alpha u_\sigma(p') \\
&\quad \cdot [g^{\mu\nu}(\underbrace{p-q}_{a})^\rho + g^{\nu\rho}(\underbrace{q+k_s}_{b})^\mu - g^{\rho\mu}(\underbrace{k_s+p}_{c})^\nu] \\
&\quad \cdot [g^{\beta\delta}(p-q)^\alpha + g^{\delta\alpha}(q+k_s)^\beta - g^{\alpha\beta}(k_s+p)^\delta] && (145)\\
&= \frac{1}{4}\frac{1}{8^2}\frac{g_s^4}{s^2} tr[f^{abc}t^c t^{c'} f^{abc'\dagger}] tr[\not{p}'\gamma_\rho \not{q}'\gamma_\alpha] \\
&\quad [g^{\mu\nu}a^\rho + g^{\nu\rho}b^\mu - g^{\rho\mu}c^\nu][g_{\mu\nu}a^\alpha + g_\nu{}^\alpha b_\mu - g^\alpha_\mu c_\nu] && (146)\\
&= \frac{3}{8^2}\frac{g_s^4}{s^2} tr[\not{p}'\gamma_\rho \not{q}'\gamma_\alpha][4a^\rho a^\alpha + a^\rho b^\alpha - a^\rho c^\alpha \\
&\quad + b^\rho a^\alpha + g^{\rho\alpha}b^2 - b^\alpha c^\rho - c^\rho a^\alpha - c^\alpha b^\rho + g^{\rho\alpha}c^2] && (147)\\
&= \frac{3}{8^2}\frac{g_s^4}{s^2} tr[\not{p}'\gamma_\rho \not{q}'\gamma_\alpha][8(qp)g^{\rho\alpha} - 2(p^\rho p^\alpha + q^\rho q^\alpha) \\
&\quad - 7(p^\rho q^\alpha + q^\rho p^\alpha)] && (148)\\
\overline{|\mathfrak{M}_s|^2} &= \frac{3}{8}\frac{g_s^4}{s^2}\left[-2(u^2+t^2) - \frac{3}{2}ut\right] && (149)
\end{aligned}$$

B.6.3 $\overline{|\mathfrak{M}_{tu}|^2}$

$$\begin{aligned}
\overline{|\mathfrak{M}_{tu}|^2} &= 2Re\overline{|\mathfrak{M}_t\mathfrak{M}_u^*|} && (150)\\
&= 2Re\left\{\frac{1}{4}\frac{1}{8^2}\frac{g_s^4}{tu}\sum \varepsilon_\lambda^\mu \varepsilon_{\lambda'}^\nu \varepsilon_\lambda^{\beta *} \varepsilon_{\lambda'}^{\alpha *} t^a t^b t^a t^b \right. \\
&\quad \left. \bar{u}_\sigma(p')\gamma_\mu \not{k}_t \gamma_\nu v_{\sigma'}(q')\bar{v}_{\sigma'}(q')\gamma_\beta(-\not{k}_u)\gamma_\alpha u_\sigma(p')\right\} && (151)\\
&= \frac{-1}{2}\frac{1}{8^2}\frac{g_s^4}{tu} tr(t^a t^b t^a t^b) tr(\not{p}'\gamma_\mu \not{k}_t \gamma_\nu \not{q}'\gamma^\mu \not{k}_u \gamma^\nu) && (152)\\
&= \frac{-4}{3}\frac{1}{8^2}\frac{g_s^4}{tu} tr[\not{p}'\not{k}_t \not{k}_u \not{q}' - \not{p}'\not{k}_u \not{q}'\not{k}_t + (k_t\cdot q')\not{p}'\not{k}_u] && (153)\\
&= \frac{-1}{12}\frac{g_s^4}{tu}\left[\frac{1}{2}tu - \frac{1}{4}tu - \frac{1}{4}tu\right] && (154)\\
\overline{|\mathfrak{M}_{tu}|^2} &= 0 && (155)
\end{aligned}$$

B.6.4 $\overline{|\mathfrak{M}_{ts}|^2}$

$$\begin{aligned}
\overline{|\mathfrak{M}_{ts}|^2} &= 2Re\overline{|\mathfrak{M}_t\mathfrak{M}_s^*|} && (156)\\
&= 2Re\left\{\frac{1}{4}\frac{1}{8^2}\frac{-ig_s^4}{ts}\sum \varepsilon_\lambda^\mu\varepsilon_{\lambda'}^\nu\varepsilon_\lambda^{\beta*}\varepsilon_{\lambda'}^{\delta*}t^a t^b t^c f^{abc\dagger}\right.\\
&\quad \cdot\bar{u}_\sigma(p')\gamma_\mu \not{k}_t\gamma_\nu v_{\sigma'}(q')\bar{v}_{\sigma'}(q')\gamma_\alpha u_\sigma(p')\\
&\quad \left.\cdot[g^{\beta\delta}(\underbrace{p-q}_{a})^\alpha + g^{\delta\alpha}(\underbrace{q+k_s}_{b})^\beta - g^{\alpha\beta}(\underbrace{k_s+p}_{c})^\delta]\right\} && (157)\\
&= \frac{1}{2}\frac{1}{8^2}\frac{g_s^4}{ts}Re\left\{-i\,tr[t^a t^b t^c f^{abc\dagger}]\right.\\
&\quad \left.\cdot tr\left[\not{p}'\gamma_\mu\not{k}_t\gamma_\nu\not{q}'\gamma^\alpha(g^{\mu\nu}a_\alpha + g^\nu{}_\alpha b^\mu - g_\alpha{}^\mu c^\nu)\right]\right\} && (158)\\
&= \frac{-6}{8^2}\frac{g_s^4}{ts}tr[\not{p}'\not{k}_t\not{q}'\not{a} + \not{p}'\not{b}\not{k}_t\not{q}' - \not{p}'\not{q}'\not{c}\not{k}_t] && (159)\\
\overline{|\mathfrak{M}_{ts}|^2} &= -\frac{3}{8}g_s^4\frac{ts}{s^2} && (160)
\end{aligned}$$

B.6.5 $\overline{|\mathfrak{M}_{su}|^2}$

$$\begin{aligned}
\overline{|\mathfrak{M}_{su}|^2} &= 2Re\overline{|\mathfrak{M}_s\mathfrak{M}_u^*|} && (161)\\
\overline{|\mathfrak{M}_{su}|^2} &= 2Re\overline{|\mathfrak{M}_u\mathfrak{M}_s^*|} && (162)\\
&= 2Re\left\{\frac{1}{4}\frac{1}{8^2}\frac{-ig_s^4}{us}\sum \varepsilon_\lambda^\mu\varepsilon_{\lambda'}^\nu\varepsilon_\lambda^{\beta*}\varepsilon_{\lambda'}^{\delta*}t^b t^a t^c f^{abc\dagger}\right.\\
&\quad \cdot\bar{u}_\sigma(p')\gamma_\mu(-\not{k}_u)\gamma_\nu v_{\sigma'}(q')\bar{v}_{\sigma'}(q')\gamma_\alpha u_\sigma(p')\\
&\quad \left.\cdot[g^{\beta\delta}(\underbrace{p-q}_{a})^\alpha + g^{\delta\alpha}(\underbrace{q+k_s}_{b})^\beta - g^{\alpha\beta}(\underbrace{k_s+p}_{c})^\delta]\right\} && (163)\\
&= \frac{1}{2}\frac{1}{8^2}\frac{g_s^4}{us}Re\left\{i\,tr[t^b t^a t^c f^{abc\dagger}]\right.\\
&\quad \left.\cdot tr\left[\not{p}'\gamma_\mu\not{k}_u\gamma_\nu\not{q}'\gamma^\alpha(g^{\mu\nu}a_\alpha + g^\nu{}_\alpha b^\mu - g_\alpha{}^\mu c^\nu)\right]\right\} && (164)\\
&= \frac{6}{8^2}\frac{g_s^4}{us}tr[\not{p}'\not{k}_u\not{q}'\not{a} + \not{p}'\not{b}\not{k}_u\not{q}' - \not{p}'\not{q}'\not{c}\not{k}_u] && (165)\\
\overline{|\mathfrak{M}_{su}|^2} &= -\frac{3}{8}g_s^4\frac{us}{s^2} && (166)
\end{aligned}$$

B.6.6 $\overline{|\mathfrak{M}_G|^2}$

As one can see in figure 7 on page 17 the ghost vertex function has only one momentum in it. So there are actually two ghost diagrams in our case

which are summed here.

$$\overline{|\mathfrak{M}_G|^2} = \overline{|\mathfrak{M}_{Gp}|^2} + \overline{|\mathfrak{M}_{Gq}|^2} \tag{167}$$

$$= \sum \frac{1}{4}\frac{1}{8^2}\frac{g_s^4}{s^2} f^{abc} t^b t^{b'} f^{ab'c\dagger} \left[\overline{u}_\sigma(p')\not{p}\nu_{\sigma'}(q')\overline{v}_{\sigma'}(q')\not{p}u_\sigma(p')\right.$$
$$\left. + \overline{u}_\sigma(p')\not{q}\nu_{\sigma'}(q')\overline{v}_{\sigma'}(q')\not{q}u_\sigma(p')\right] \tag{168}$$

$$= \frac{3}{8^2}\frac{g_s^4}{s^2} tr[f^{abc} t^b t^{b'} f^{ab'c\dagger}] tr[\not{p}'\not{p}\not{q}'\not{p} + \not{p}'\not{q}\not{q}'\not{q}] \tag{169}$$

$$\overline{|\mathfrak{M}_G|^2} = \frac{3}{8}\frac{g_s^4}{s^2}\frac{1}{2} tu \tag{170}$$

References

[1] T. Kalliokoski, http://www.xs4all.nl/ jcdverha/scijokes/2_1.html, (2002)

[2] E. Rutherford, The Scattering of the α and β Rays and the Structure of the Atom, Proc. Manch. Lit. and Phil. Soc. IV, 55, 18-20 (1911)

[3] Suurin tiede Kemian historia, J. Hudson, Art House, 1995. Original: The History of Chemistry, Chapman and Hall, (1992)

[4] J. J. Thomson, Phil. Mag. 44, 293 (1897)

[5] N. Bohr, Phil. Mag. 26, 1; 476; 857 (1913)

[6] P. A. M. Dirac, The quantum theory of the electron, Proc. R. Soc. (London) A 117 610-612, part II 118 351-361 (1928)

[7] Murray Gell-Mann, A schematic model of baryons and mesons, Phys.Lett.8:214-215 (1964)

[8] R. Feynman, Phys. Rev. Lett. 23, 1415 (1969)

[9] J. D. Bjorken & E. A. Paschos, Phys. Rev. 185, 1975 (1969)

[10] G. Goldhaber, et. al., Phys. Rev. Lett.37:255-259 (1976)

[11] A. Smith, eConf C020629:THAT05 (2002)

[12] H. J. Lipkin, Nucl.Phys.Proc.Suppl.115:117-121 (2003) Phys. Rev. 112, 1344-1360 (1958)

[13] F. J. Gilman,Phys. Rep. 4C No. 3 (1972)

[14] For example: V. P. Gonçalves and M. V. T. Machado,Phys. Rev. D 71, 014025 (2005)

[15] For example: I. V. Anikin, B. Pire, L. Szymanowski, O. V. Teryaev and S. Wallon,Phys. Rev. D 71, 034021 (2005)

[16] F. Halzen & A. D. Martin, Quarks & Leptons: An Introductory Course in Modern Particle Physics, John Wiley & Sons, (1984)

[17] J. D. Bjorken, Asymptotic Sum Rules at Infinite Momentum, Phys. Rev. 179, 1547 (1969)

[18] J. I. Friedman,Rev. mod. phys. 63:615 (1991)

[19] G. Zweig, An SU_3 model for strong interaction symmetry and its breaking II. CERN preprint TH 412 (1964)

[20] I. Hinchliffe and A. Kwiatkowski,Ann. Rev. Nucl. Part. Sci. 46:609-645 (1996)

[21] H. Plothow-Besch, PDFLIB Users's Manual - Version 8.04, W5051 PDFLIB, CERN (2000)

[22] G. Altarelli and G. Parisi,Nucl. Phys. B126, 298-318, (1977)

[23] M. Hirai, S. Kumano and T.-H. Nagai,Phys. Rev. C 70, 044905, (2004)

[24] K. J. Eskola, V. J. Kolhinen, C. A. Salgado,Eur. Phys. J. C9, 61-68 (1999)

[25] H. L. Lai, et al.,Eur.Phys.J. C12:375-392, (2000)

[26] K. J. Eskola, H. Honkanen, V. J. Kolhinen, J. w. Qiu and C. A. Salgado,Nucl. Phys. B 660, (2003)

[27] G. Sterman and J. Smith, Handbook of perturbative QCD, Rev. Mod. Phys. Vol 67, No. 1, (1995)

[28] R. K. Ellis, W. J. Stirling and B. R. Webber, QCD and Collider Physics, Cambridge monographs on particle physics, nuclear physics and cosmology, (2003)

[29] S. M. Schneider, W. Greiner and G. Soff,Phys. Rev. D 46:2930-2940, (1992)

[30] W. M. Yao et al.,Journal of Physics G 33, 1, (2006)

[31] R. Vogt, S. J. Brodsky and P. Hoyer,Nucler Physics B Vol 383, 643-684, (1992)

[32] N. Carrer and A. Dainese, ALICE-INT-2003-019 v.3, (2003)

[33] N. Cabibbo,Phys. Rev. Lett. 10, (1961)

[34] M. Kobayashi and T. Maskawa, Prog. Theor. Phys. 49, (1973)

[35] David Neuffer, μ^+-μ^- Colliders, CERN 99-12, (1999)

[36] R. K. Bock and A. Vasilescu, The Particle Detector BriefBook, http://rkb.home.cern.ch/rkb/titleD.html, (1998)

[37] R. W. Assmann et. al, A 3 TeV e^+e^- Linear Collider Based on CLIC Technology, CERN 2000-008, (2000)

[38] The Large Hadron Collider: conceptual design, CERN-AC-95-05 LHC, (1995)

[39] LHC Design Report, v.1: the LHC Main Ring, CERN-2004-003-V1, (2004)

[40] ALICE: Physics Performance Report, Volume II, J. Phys. G: Nucl, part. Phys. 32, 1295-2040, (2006)

[41] LHC Design Report, v.2: the LHC Infrastructure and General Services, CERN-2004-003-V2, (2004)

[42] LHC Design Report, v.3: the LHC Injector Chain, CERN-2004-003-V3, (2004)

[43] ALICE Technical Proposal for A Large Ion Collider Experiment at the CERN LHC, CERN/LHCC/95-71, LHCC/P3, (1995)

[44] ALICE Technical Design Report of the Inner Tracking System (ITS), CERN/LHCC 99-12, ALICE TDR 4, (1999)

[45] ALICE: Physics Performance Report, Volume I, J. Phys. G: Nucl. Part. Phys. 30, 1517-1763, (2004)

[46] ALICE Technical Design Report of the Time Projection Chamber, CERN/LHCC 2000-001, ALICE TDR 7, (2000)

[47] ALICE Addendum to the Technical Design Report of the Time of Flight System (TOF), CERN/LHCC 20002-016, Addendum to ALICE TDR 8, (2002)

[48] E. C. Zeballos, I. Crotty, D.Hatzifotiadou, J. L. Valverde, S. Neupane, M. C. S. Williams, A. Zichichi, Nucl. Instr. Meth. A374, 132, (1996)

[49] M. E. Peskin and D. V. Schroeder, An Introduction to Quantum Field Theory, Perseus Books, (1995)

[50] T. Sjöstrand, S. Mrenna and P. Skands, PYTHIA 6.4 Physics and Manual, LU TP 06-13, FERMILAB-PUB-06-052-CD-T, (2006)

[51] I. Peruzzi, et. al, Phys.Rev.Lett.37, (1976)

[52] S. Mandelstam, Phys. Rev. 112, 1344-1360 (1958)